SUPPORTING INFORMATION

Intramolecular Hydrogen Bond-Driven Conformational Preferences in Pyridine Containing Dibenzamide and Dicarboxamide Derivatives: Evidence From NMR and DFT-Based Computation

Swaraj Pathak[a], Sandeep Kumar Mishra[b*], Nilamoni Nath[a*]

[a]Department of Chemistry, Gauhati University, Guwahati, Assam-781014, India

[b]Department of Physics and NMR Research Centre, Indian Institute of Science Education and Research, Pune 411008, India

*Corresponding author's E-mail id:

sandeepmishra@iiserpune.ac.in

nilamoni.nath@gmail.com

Table of Contents **Pages**

List of Figures

Methods

Experimental methods:

All the NMR experiments were performed at a 400 MHz Bruker Ascend^{TM} spectrometer. Two-dimensional NMR experiments such as ^{1}H-^{19}F HOESY[1, 2] and ^{1}H-^{15}N HSQC[3] were performed using standard pulse sequences available in the Bruker library. The synthesis of all the molecules investigated in this study were synthesized following the procedure.

General procedure for synthesis of the A and B series of molecules:

Synthesis procedure for A series:

High-purity, commercially available reactants were purchased and employed without any additional purification. Thionyl chloride ($SOCl_2$, 30 mmol) was added to the respective acid derivatives (2.5 mmol) in dry CH_2Cl_2, and the resulting suspension was refluxed under a nitrogen atmosphere overnight at 40°C. After completion of the reaction, the excess $SOCl_2$ was evaporated under reduced pressure. The acid chloride was dissolved in dry CH_2Cl_2 and cooled to 0°C. A solution containing triethylamine(2 mmol) and 2,6-diaminopyridine (1 mmol) in dry CH_2Cl_2 was added dropwise to the reaction mixture, which was then stirred at 0°C for 30 minutes and subsequently at room temperature for 16 hours under a nitrogen atmosphere. Further, the suspension was washed with a saturated aqueous mixture of NH_4Cl and water, then dried over anhydrous Na_2SO_4 and concentrated *in vacuo*. The crude product was purified with column chromatography using an ethyl acetate/petroleum ether solvent mixture with a polarity gradient.

The reaction scheme for the synthetic procedure is shown below.

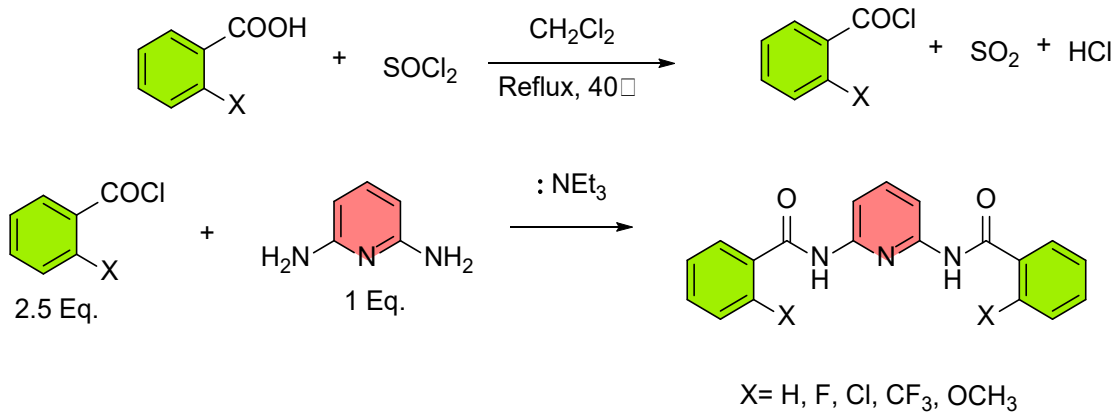

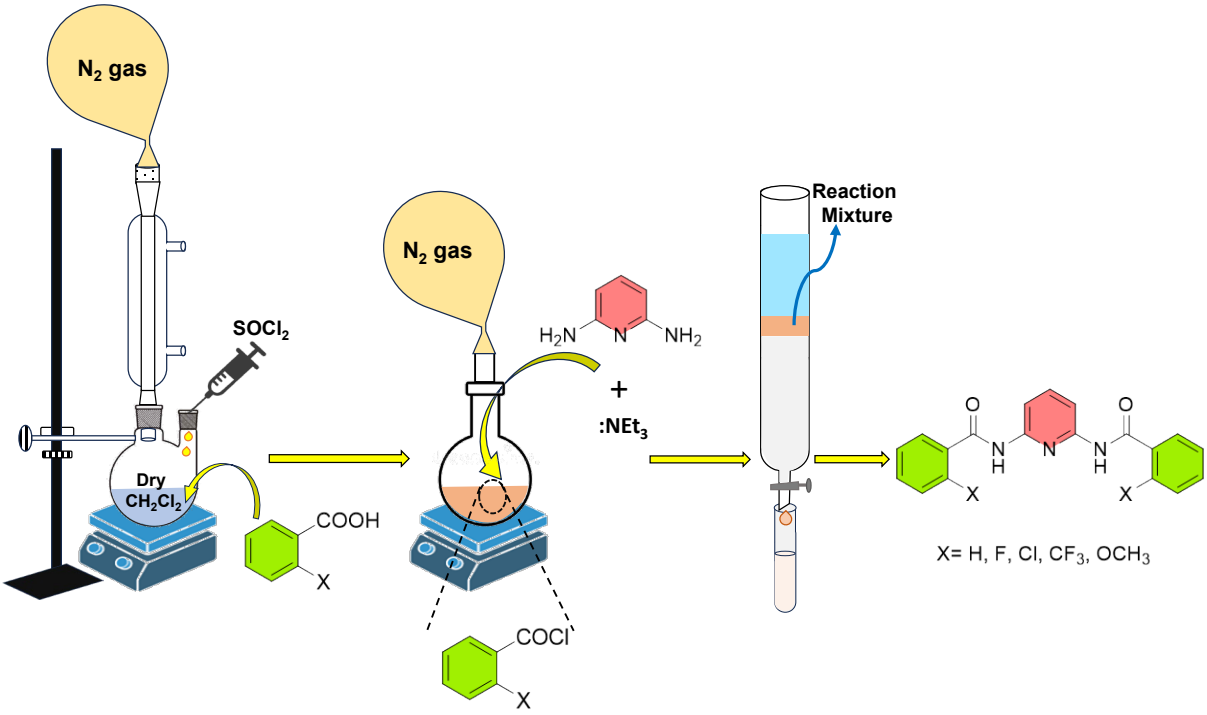

Scheme S1: Chemical and graphical representation of the synthetic procedure for the series A molecules.

Synthesis procedure for B series:

The 2,6-dipicollinic acid (1mmol) was treated with thionyl chloride ($SOCl_2$, 30 mmol) in acetonitrile and refluxed under a nitrogen atmosphere overnight at 80°C. Upon completion of the reaction, excess thionyl chloride was removed *in vacuo*, resultant acid chloride was dissolved in dry CH_2Cl_2 and cooled to 0°C. A solution of triethylamine(2 mmol) and desired amine derivatives(2.5 mmol) in dry CH_2Cl_2 was added dropwise, then stirred 30 minutes at 0°C and subsequently at room temperature for 16 hours under a nitrogen atmosphere. The reaction mixture was washed with a saturated solution of NH_4Cl and water, dried over anhydrous Na_2SO_4, and concentrated under reduced pressure. The crude product was purified by column chromatography using an ethyl acetate/petroleum ether solvent mixture with a polarity gradient.

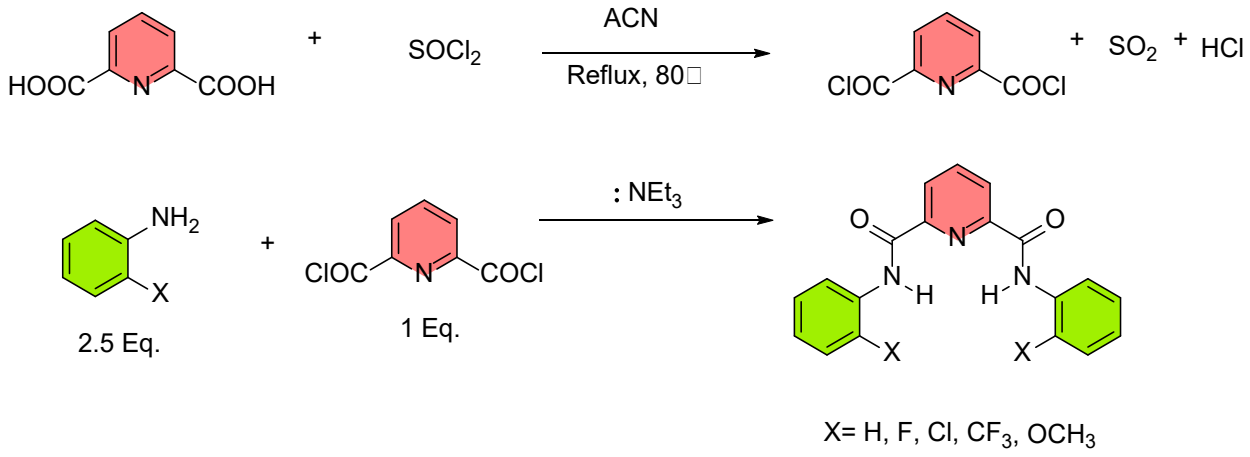

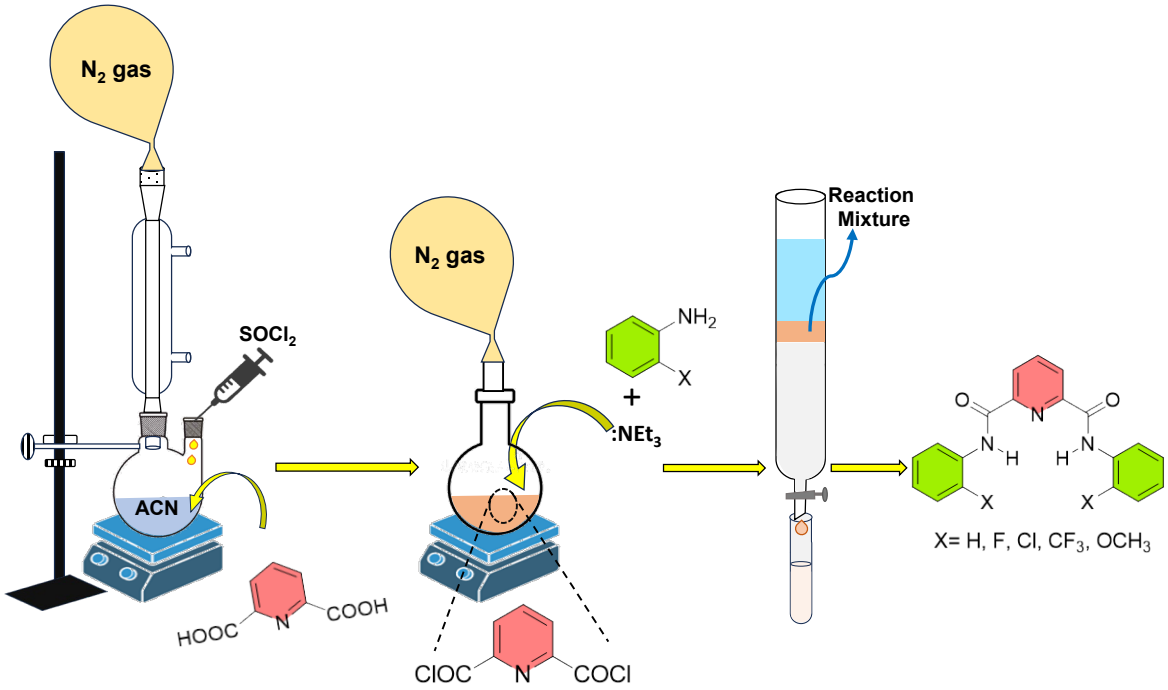

Scheme S2: Chemical and graphical representation of the synthetic procedure for the series B molecules.

Computational methods:

All molecular mechanics calculations were carried out in the *Gaussian 16* software.[4] The 3D structures of all the molecules listed in Scheme 1 were generated using GaussView software. The structures were then set for geometry optimization and frequency calculation using B3LYP/6-311+G(d,p) and B3LYP/6-311++G(d,p) basis set of DFT with chloroform as solvation medium modeled using integral equation formalism-polarizable continuum model (IEF-PCM).[5] The wave function (.wfn) files were derived from the optimized minimum energy structures and subsequently used for QTAIM and NCI analyses. Different DFT levels of theory were employed for geometry optimization depending on the calculation type, and the specific levels used are noted in the respective sections. DFT-based NMR calculations were carried out using the Gauge-Independent Atomic Orbital (GIAO)[6] method employing the minimum energy geometries for all investigated molecules. The shielding constants obtained from DFT-based NMR calculations were converted to chemical shifts using TMS as the reference standard, following the relation, $\delta(ppm)=\sigma_{TMS}-\sigma_{theor}$. The σ_{TMS} value was determined using the same computational parameters and level of theories as applied for the investigated molecules.

The implicit solvent model (IEF-PCM) employed in this study was used for geometry optimization for QTAIM, NCI and NBO analyses, as well as for NMR calculations to predict the NH proton chemical shift in chloroform. In continuum solvation approaches such as PCM, the solvent is represented as thermally averaged, isotropic continuous electric field, where solute-solvent interactions are primarily described in terms of bulk electrostatic polarization.[7] Consequently, specific solvent-solute interactions such as hydrogen bonding between DMSO and -NH group, are not explicitly treated within the IEF-PCM framework.[7] Therefore, specific DMSO-NH interactions observed from the DMSO titration was only done experimentally and were not modelled computationally. Previous studies have shown that such HB interactions require explicit solvent treatment, which is not capture within implicit solvent model.[7, 8]

NMR Analysis

The used solvents and the spectrometer frequencies of respective nuclei for all 1D and homonuclear 2D experiments are defined in the figure captions. All the 2D heteronuclear experiments are performed at the 400 MHz ^{1}H resonating frequency.

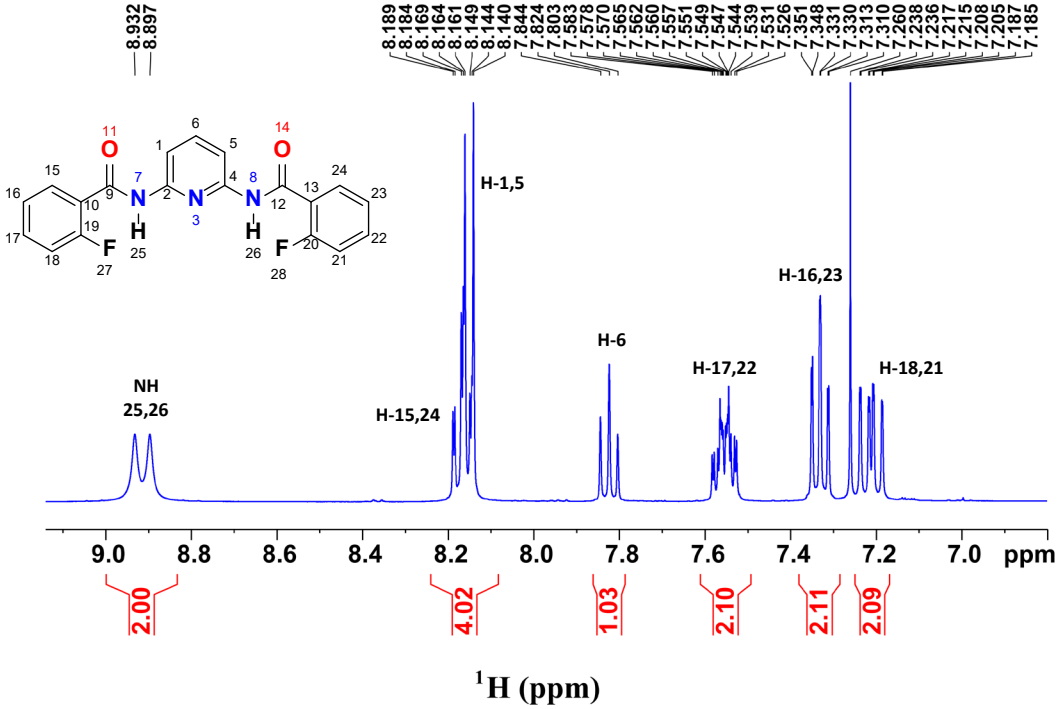

Figure S1: 400 MHz ^{1}H-NMR spectrum of A2 molecule in $CDCl_3$ solvent

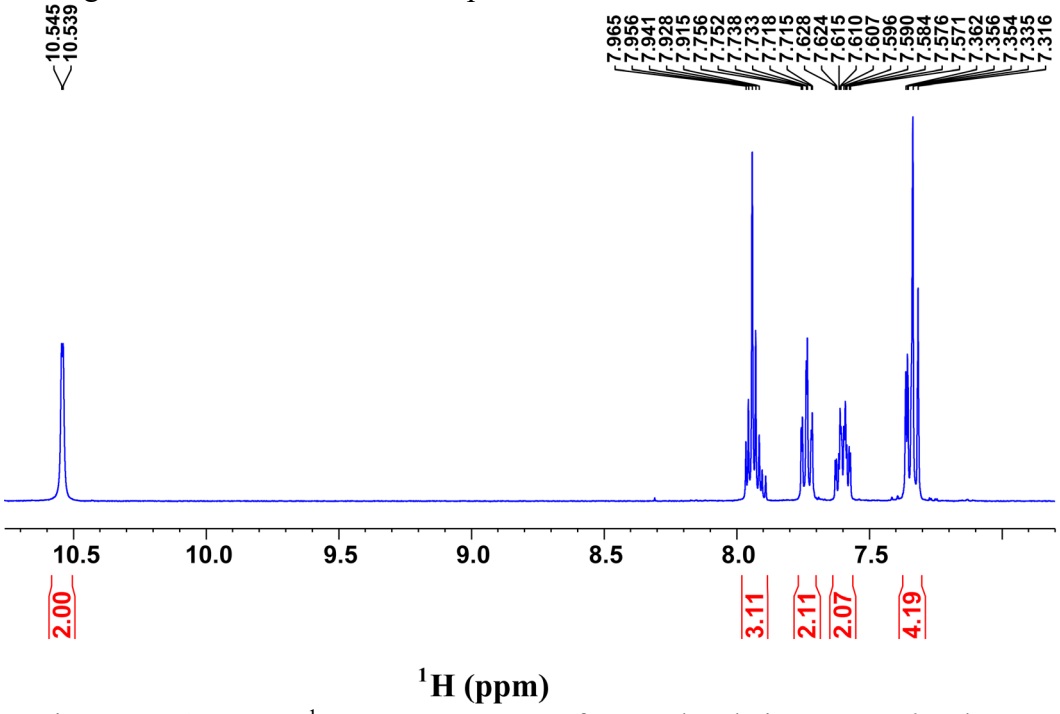

Figure S2: 400 MHz ^{1}H-NMR spectrum of A2 molecule in DMSO-d_6 solvent

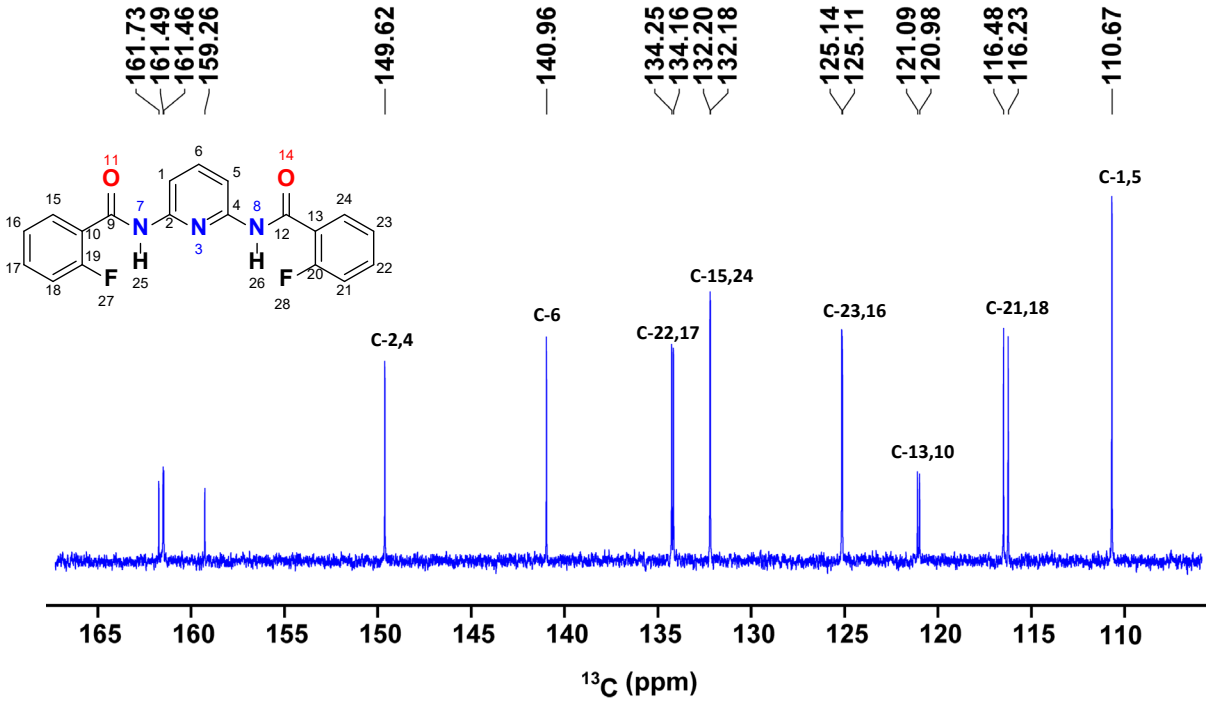

Figure S3: 100 MHz ^{13}C-NMR spectrum of the A2 molecule in $CDCl_3$ solvent.

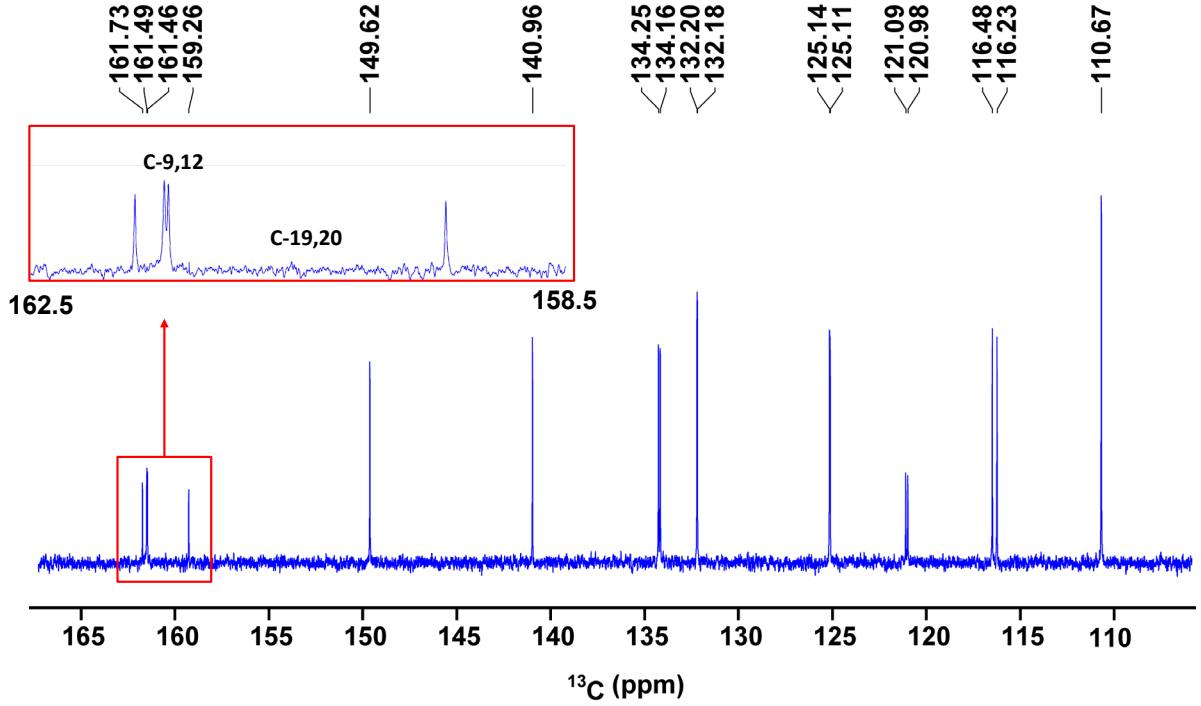

Figure S4: Expanded region of 100 MHz ^{13}C-NMR spectrum of Figure S2.

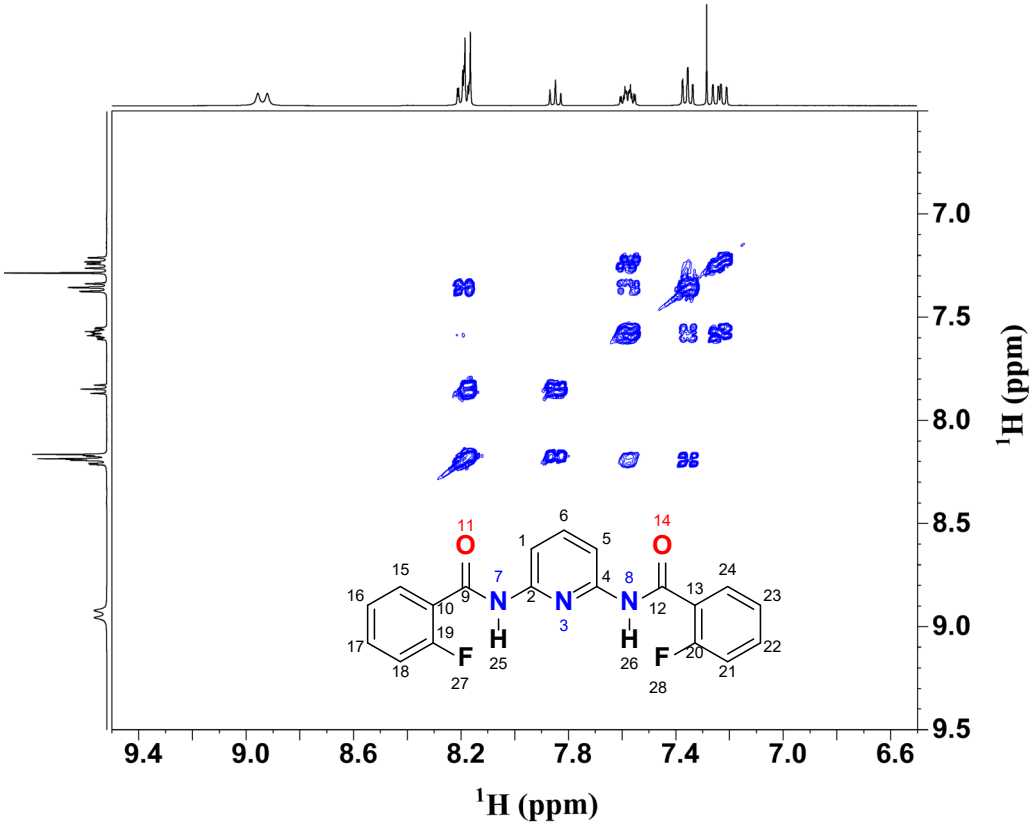

Figure S5: 2D COSY spectrum of A2 molecule measured at 400 MHz in $CDCl_3$ solvent.

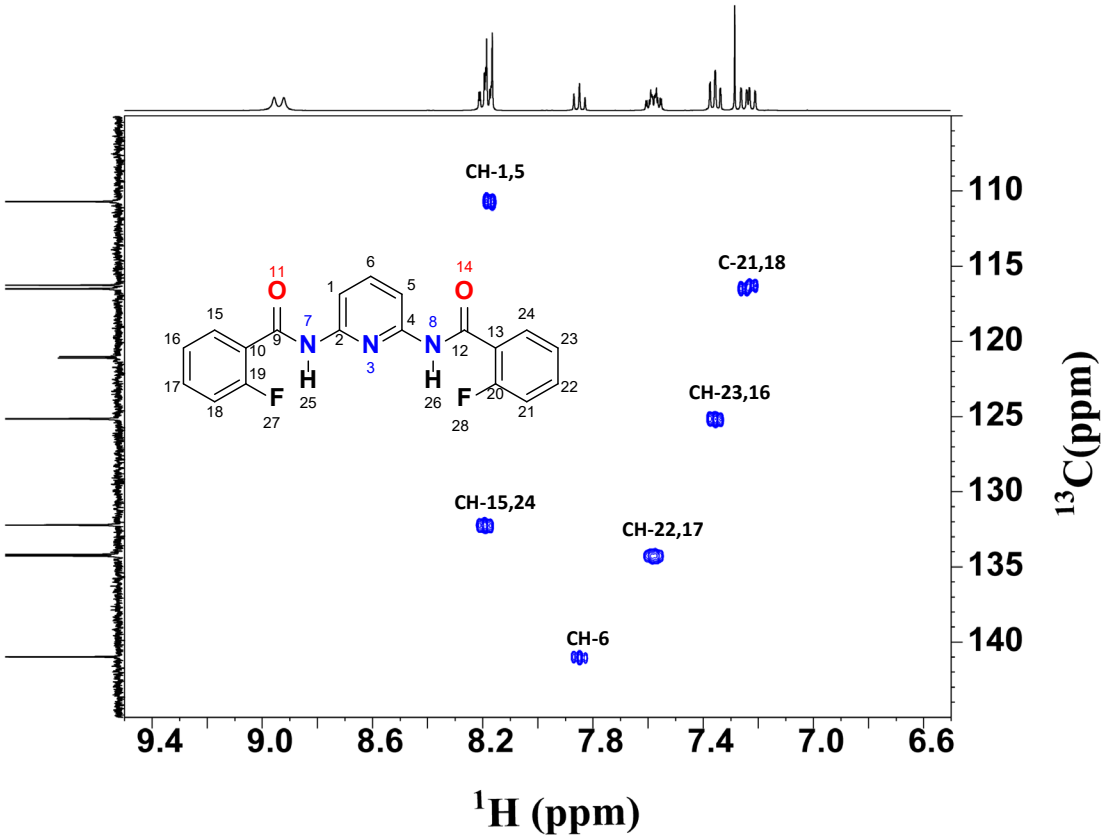

Figure S6: 2D ^{13}C-^{1}H HSQC spectrum of A2 molecule in $CDCl_3$ solvent.

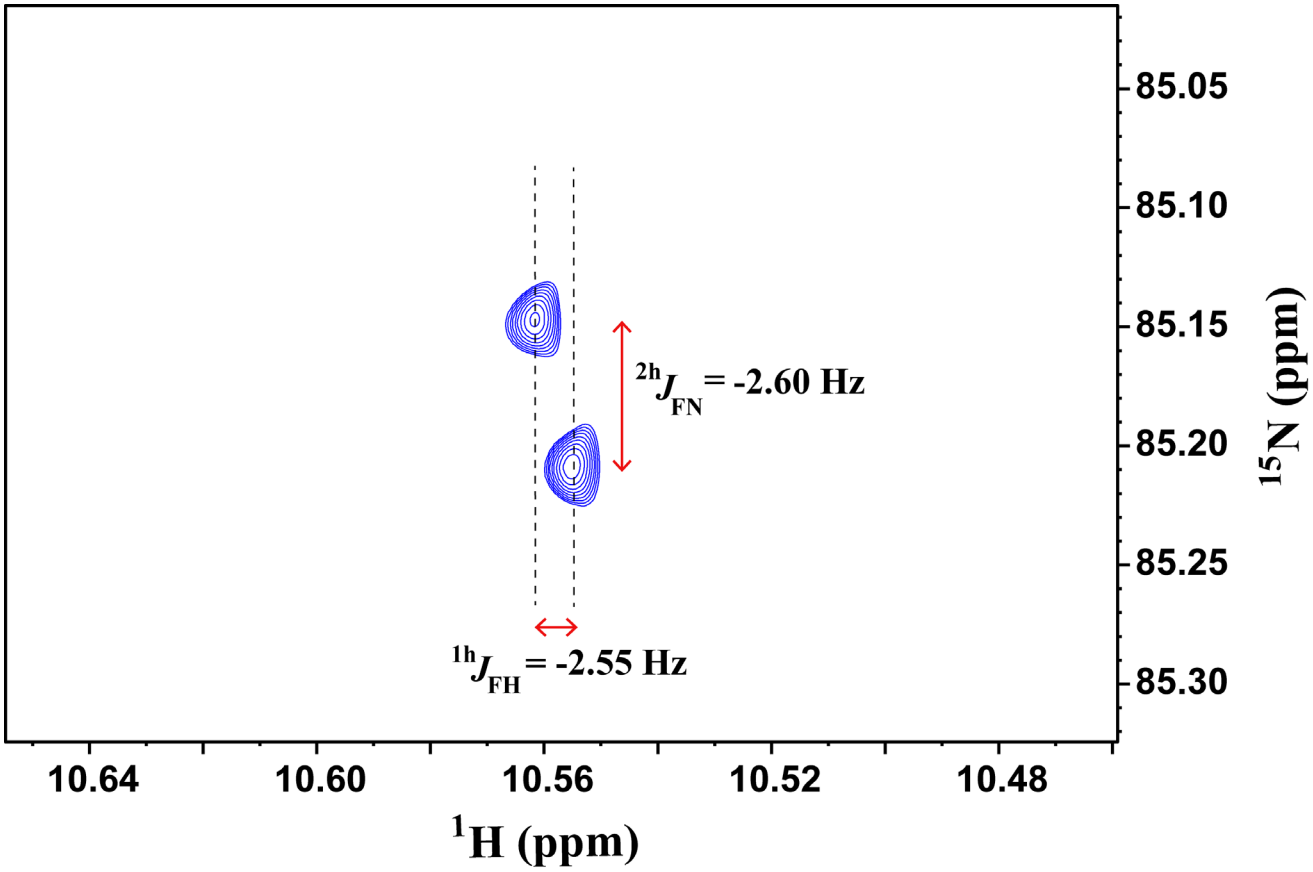

Figure S7: 2D ^{1}H-decoupled 2D ^{1}H-^{15}N HSQC spectrum of A2 molecule in DMSO-d_6 solvent

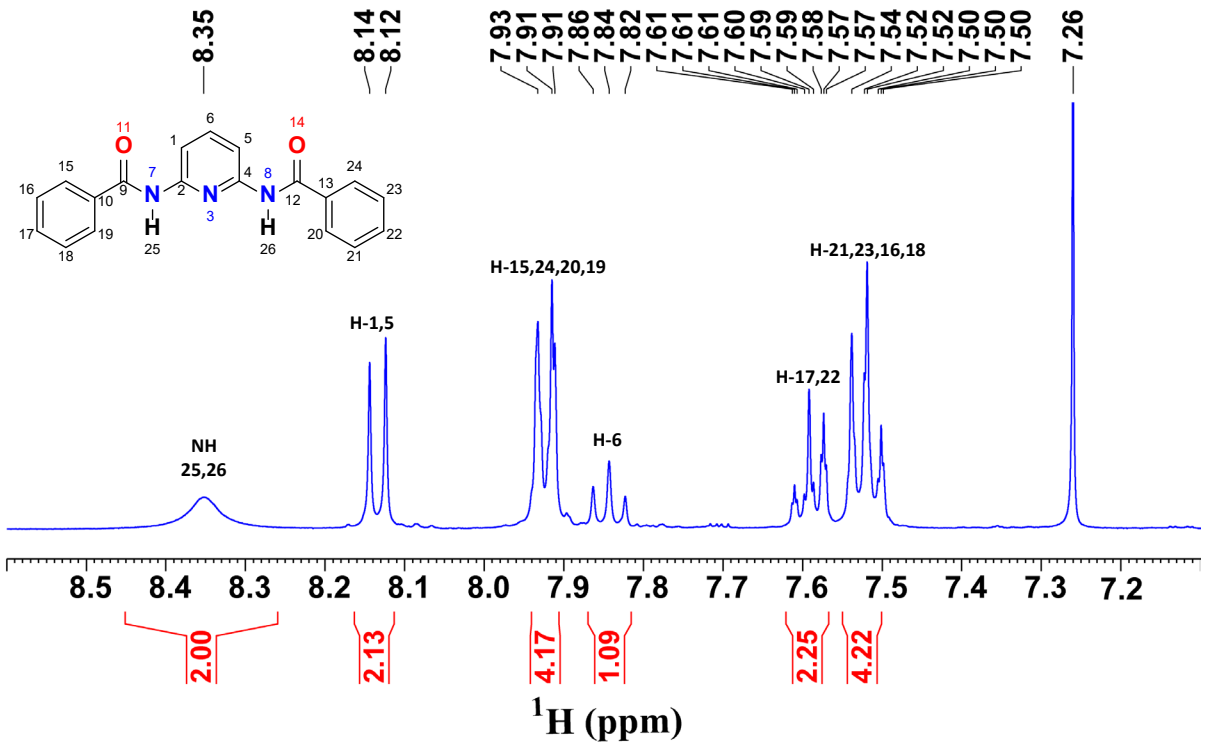

Figure S8: 400 MHz ^{1}H-NMR spectrum of A1 molecule in $CDCl_3$ solvent.

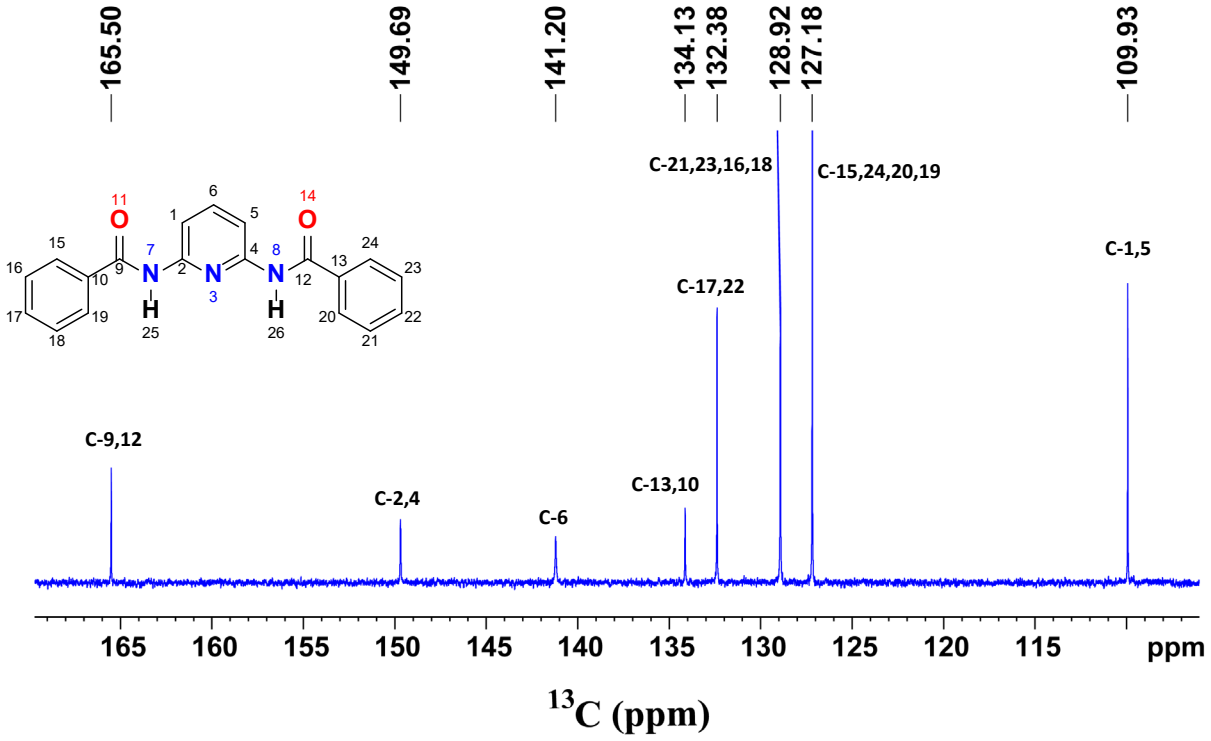

Figure S9: 100 MHz ^{13}C-NMR spectrum of A1 molecule in $CDCl_3$ solvent.

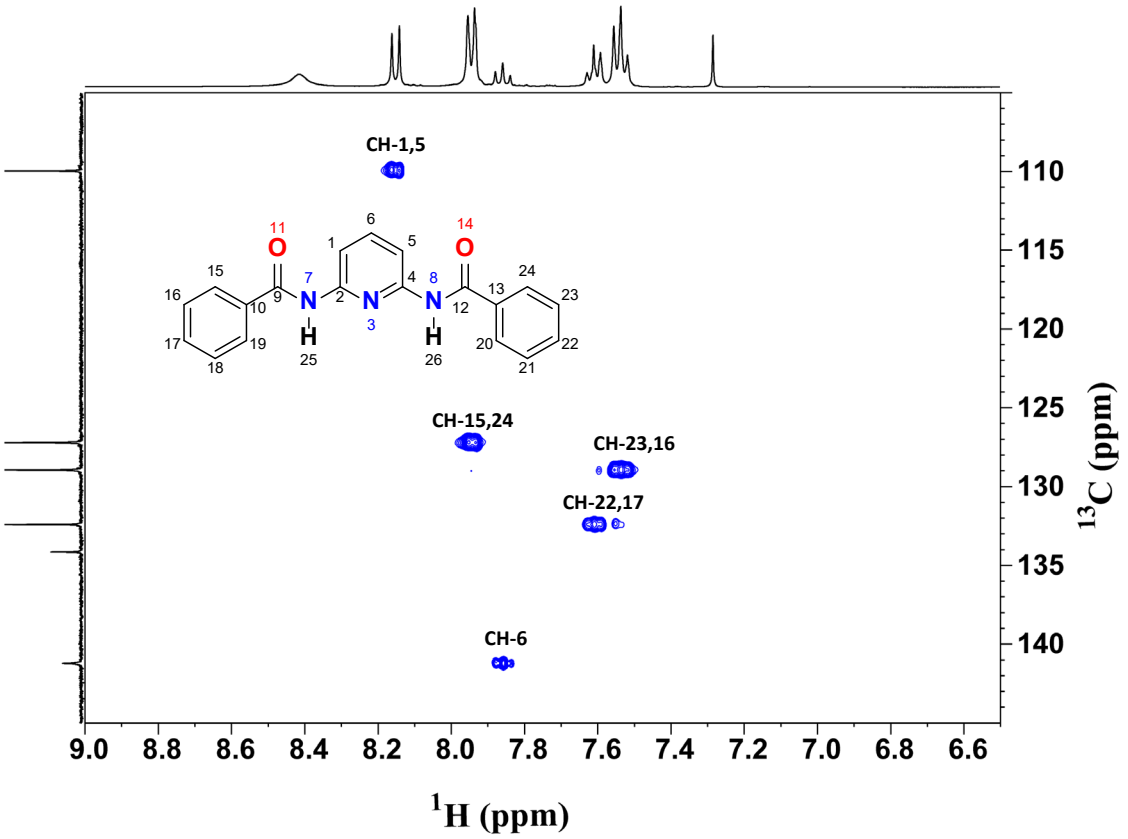

Figure S10: 2D ^{13}C-^{1}H HSQC spectrum of A1 molecule in $CDCl_3$ solvent

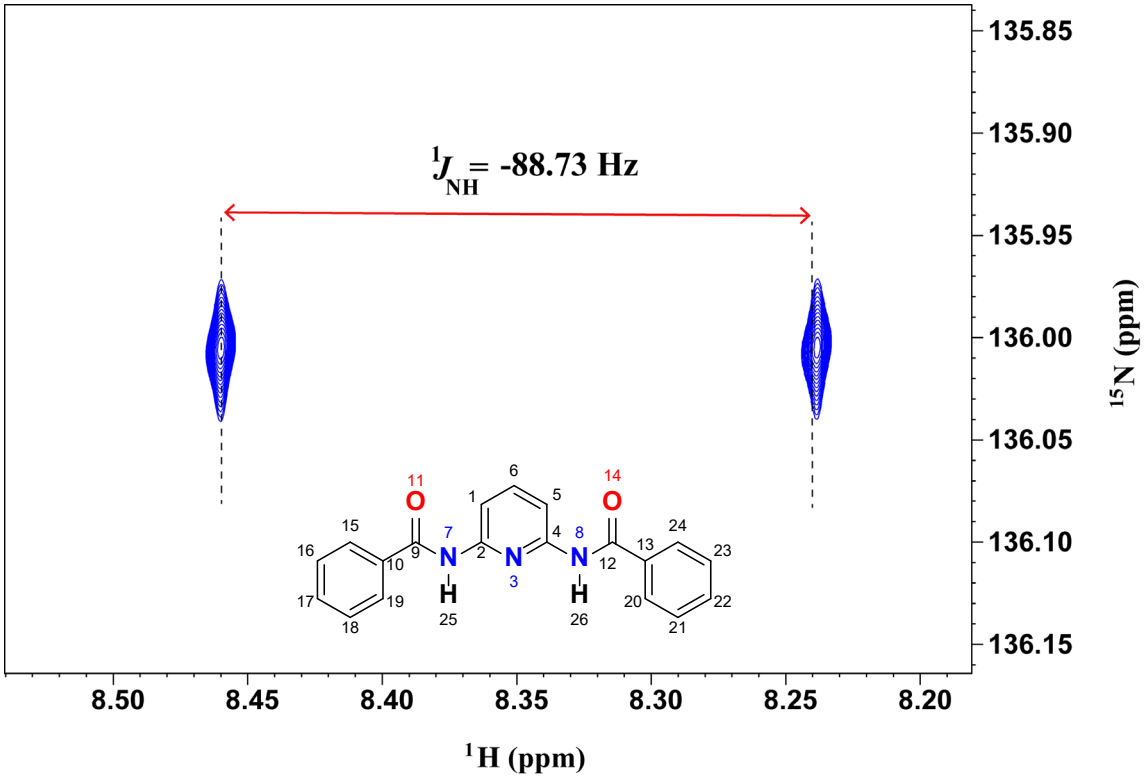

Figure S11: ^{1}H-coupled 2D ^{1}H-^{15}N HSQC spectrum of A1 molecule in $CDCl_3$ solvent.

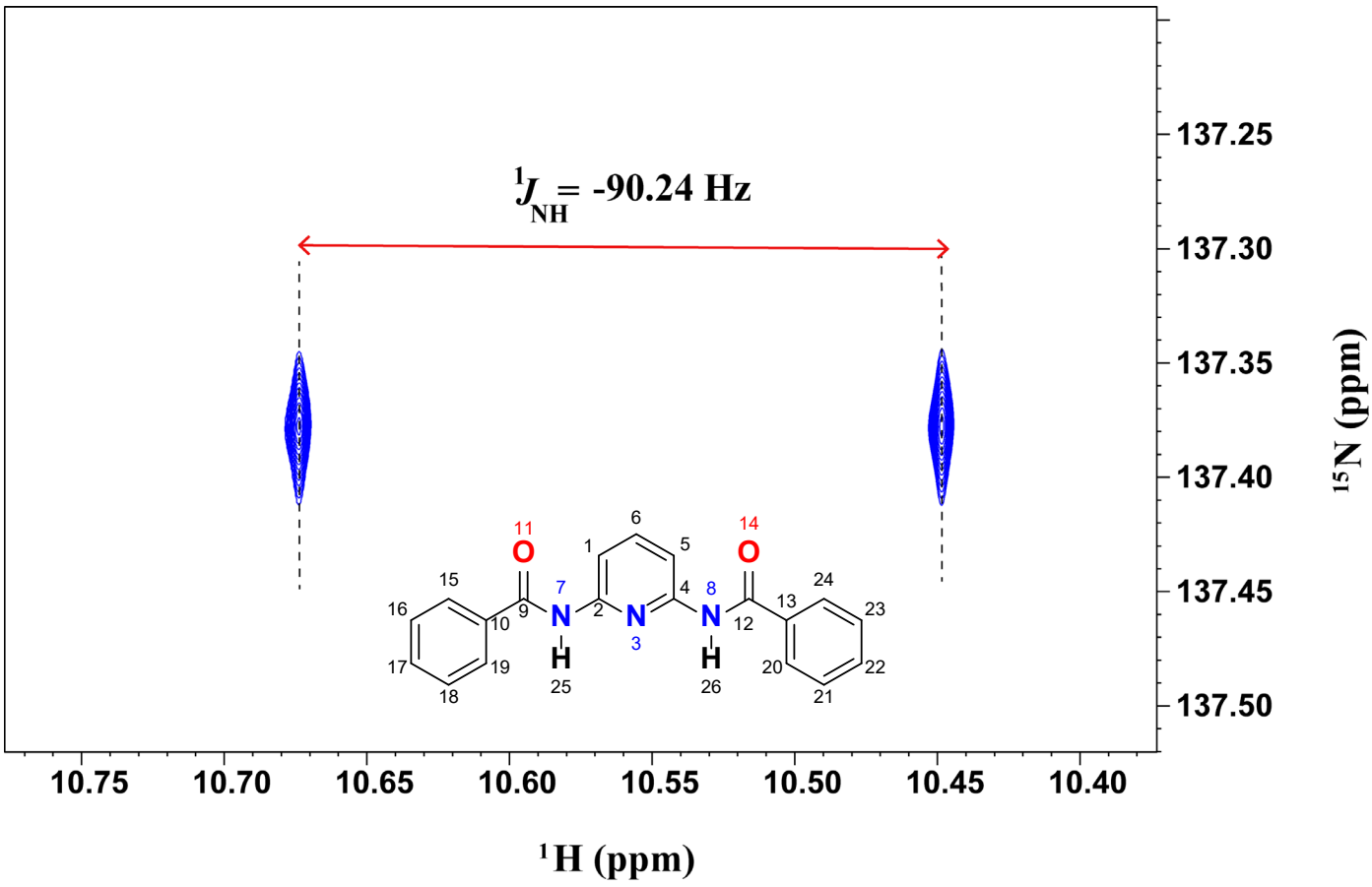

Figure S12: ^{1}H-coupled 2D ^{1}H-^{15}N HSQC spectrum of A1 molecule in DMSO-d_6 solvent.

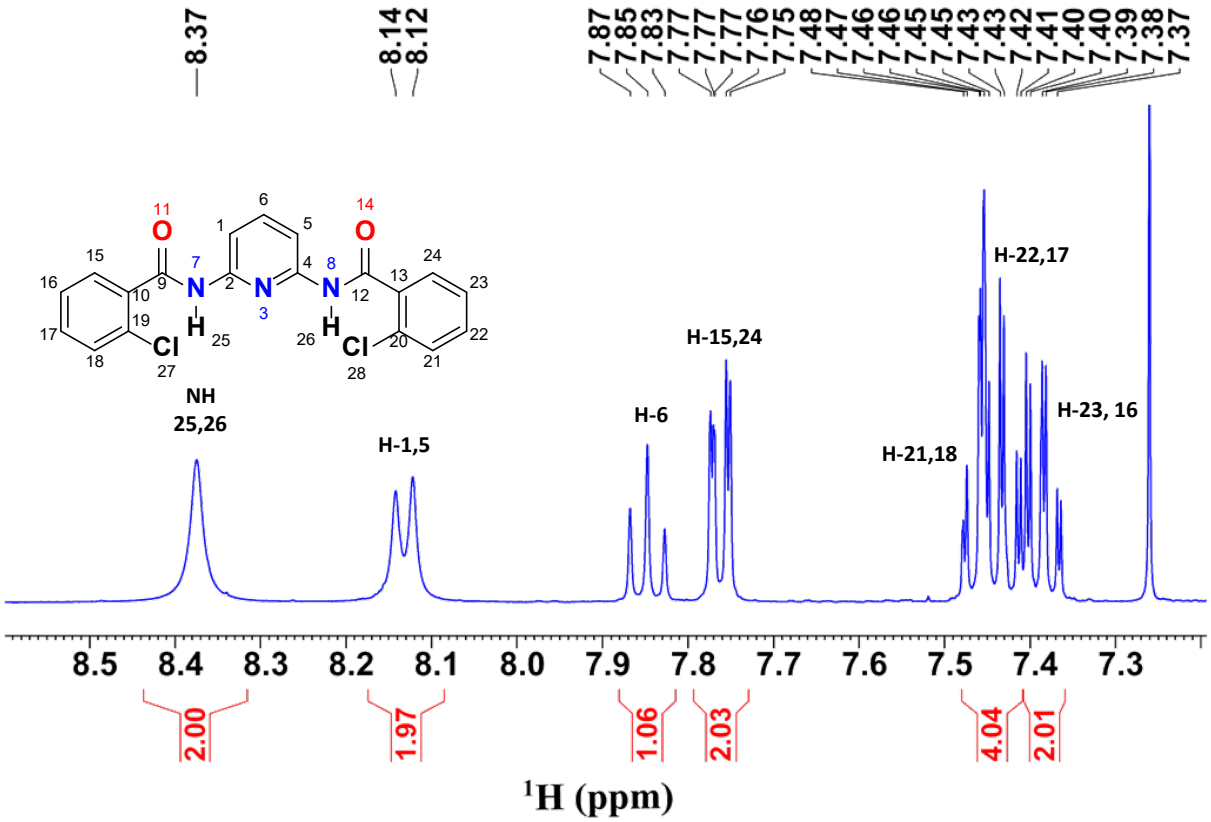

Figure S13: 400 MHz ^{1}H-NMR spectrum of A3 molecule in $CDCl_3$ solvent.

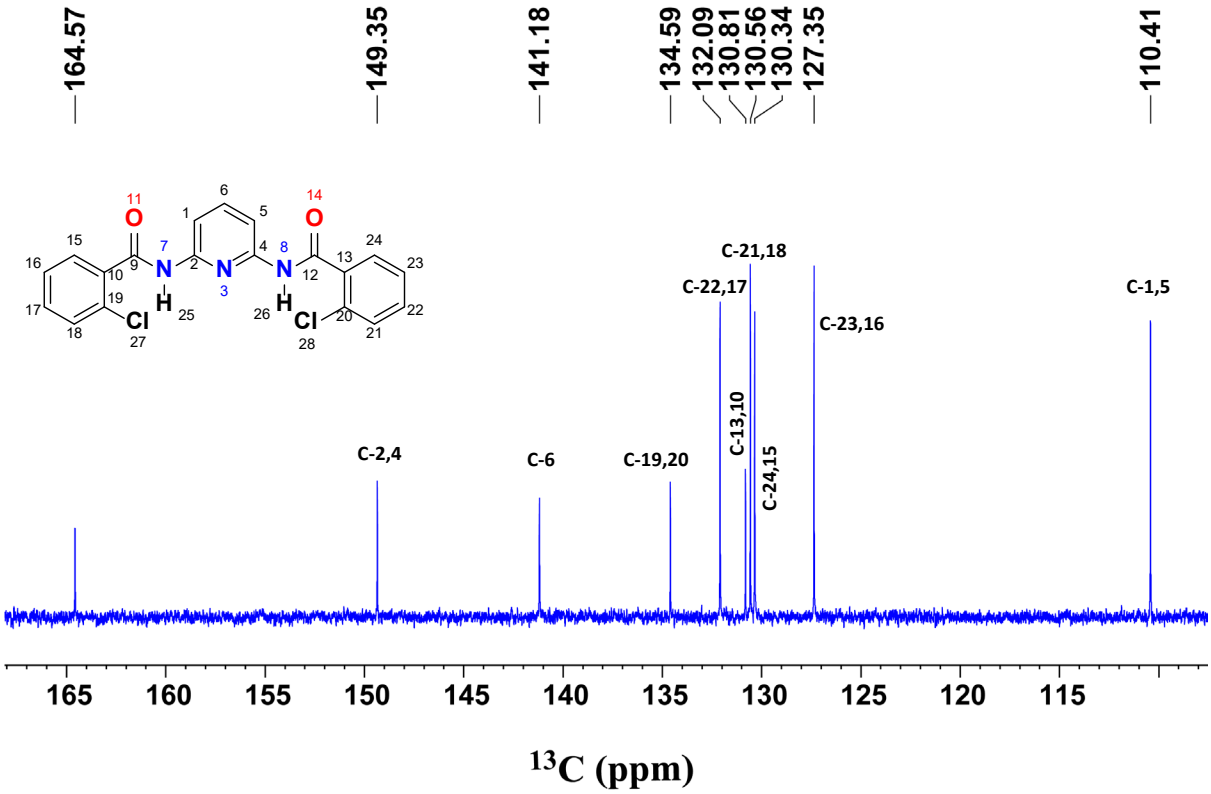

Figure S14: 100 MHz ^{13}C-NMR of A3 molecule in $CDCl_3$ solvent

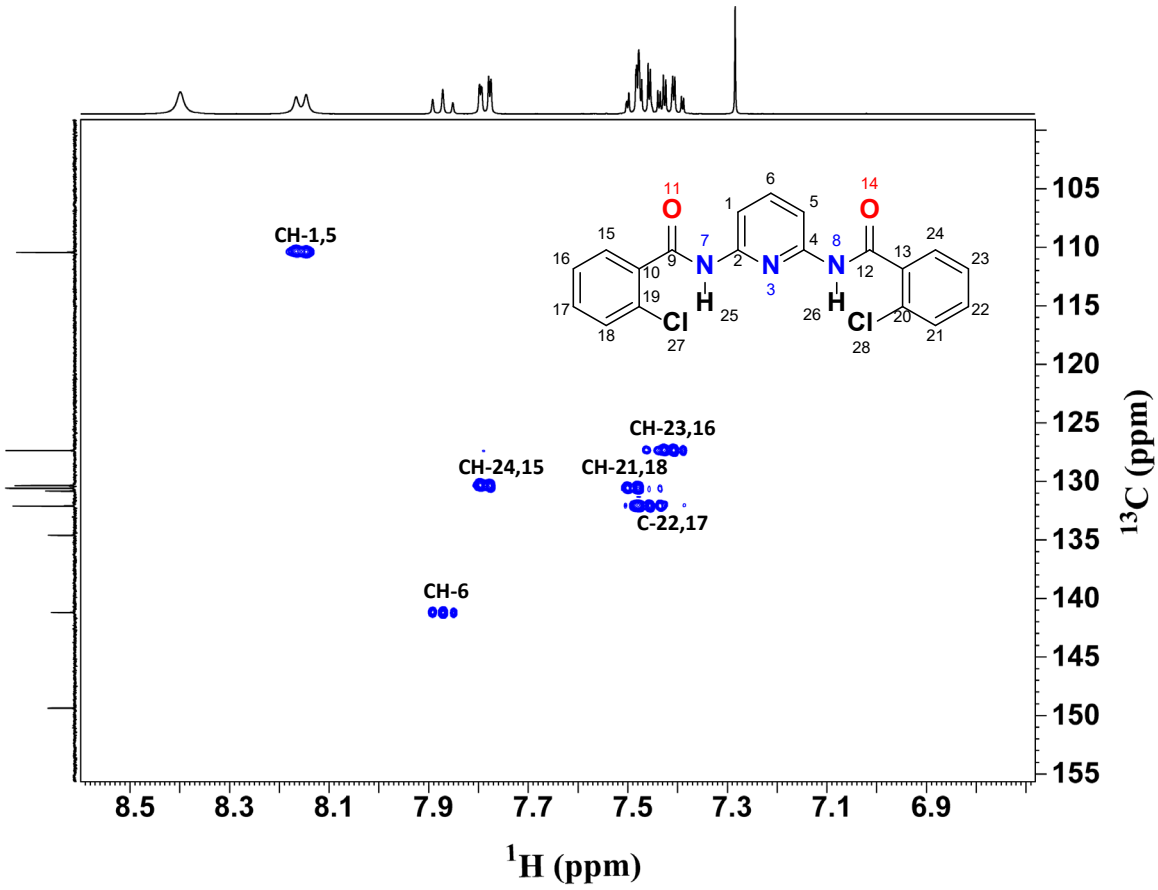

Figure S15: 2D ^{13}C-^{1}H HSQC spectrum of A3 molecule in $CDCl_3$ solvent

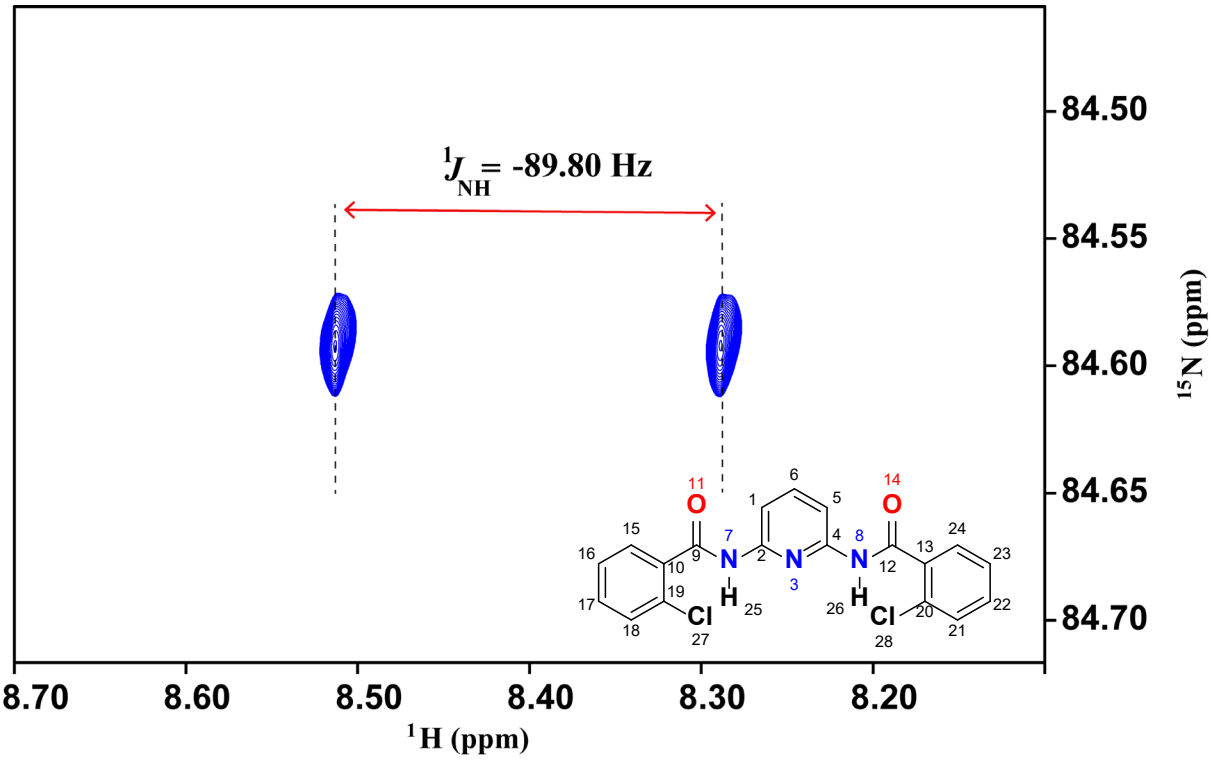

Figure S16: ^{1}H-coupled 2D ^{1}H-^{15}N HSQC spectrum of A3 molecule in $CDCl_3$ solvent.

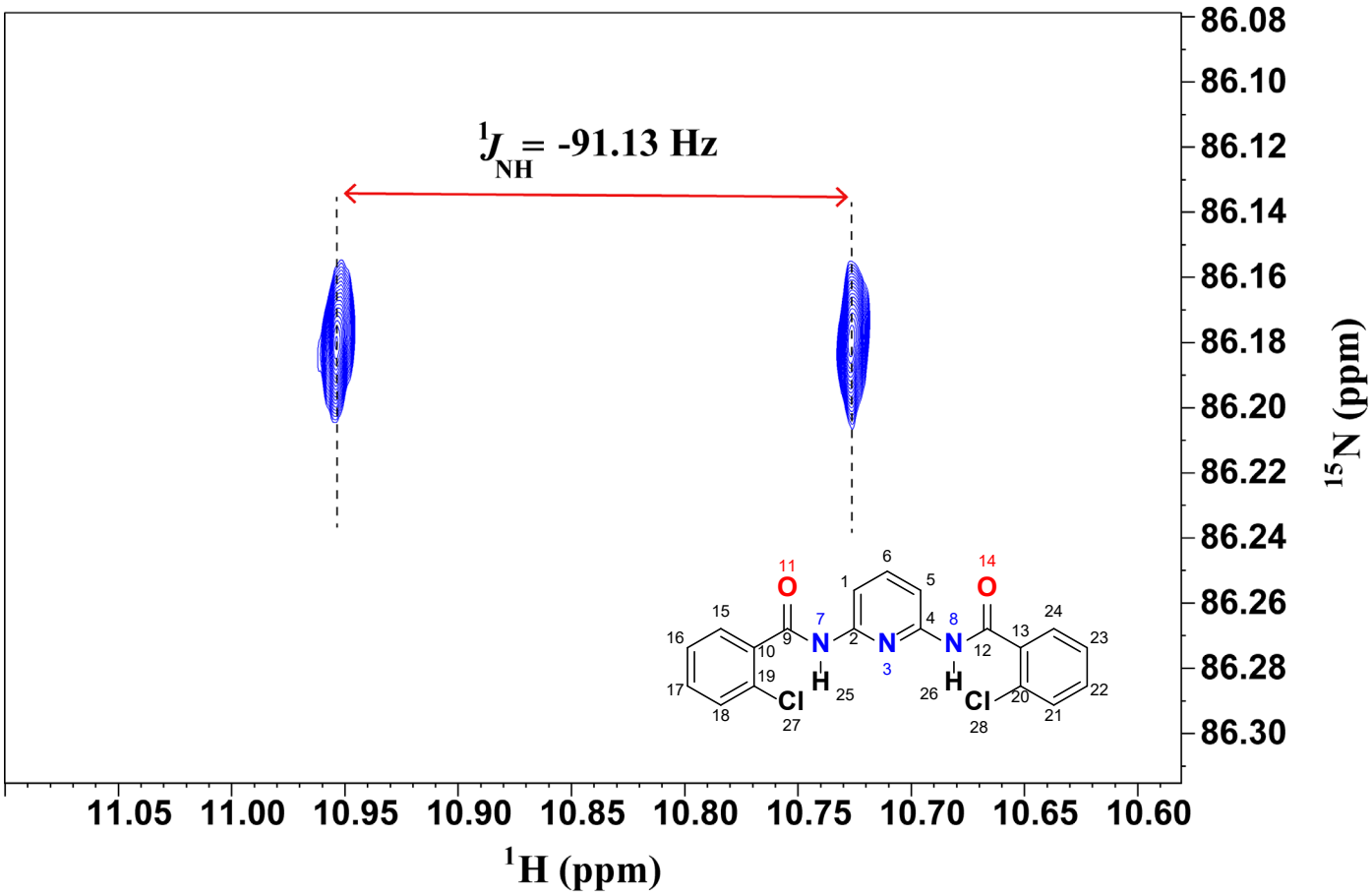

Figure S17: ^{1}H-coupled 2D ^{1}H-^{15}N HSQC spectrum of A3 molecule in DMSO-d_6 solvent.

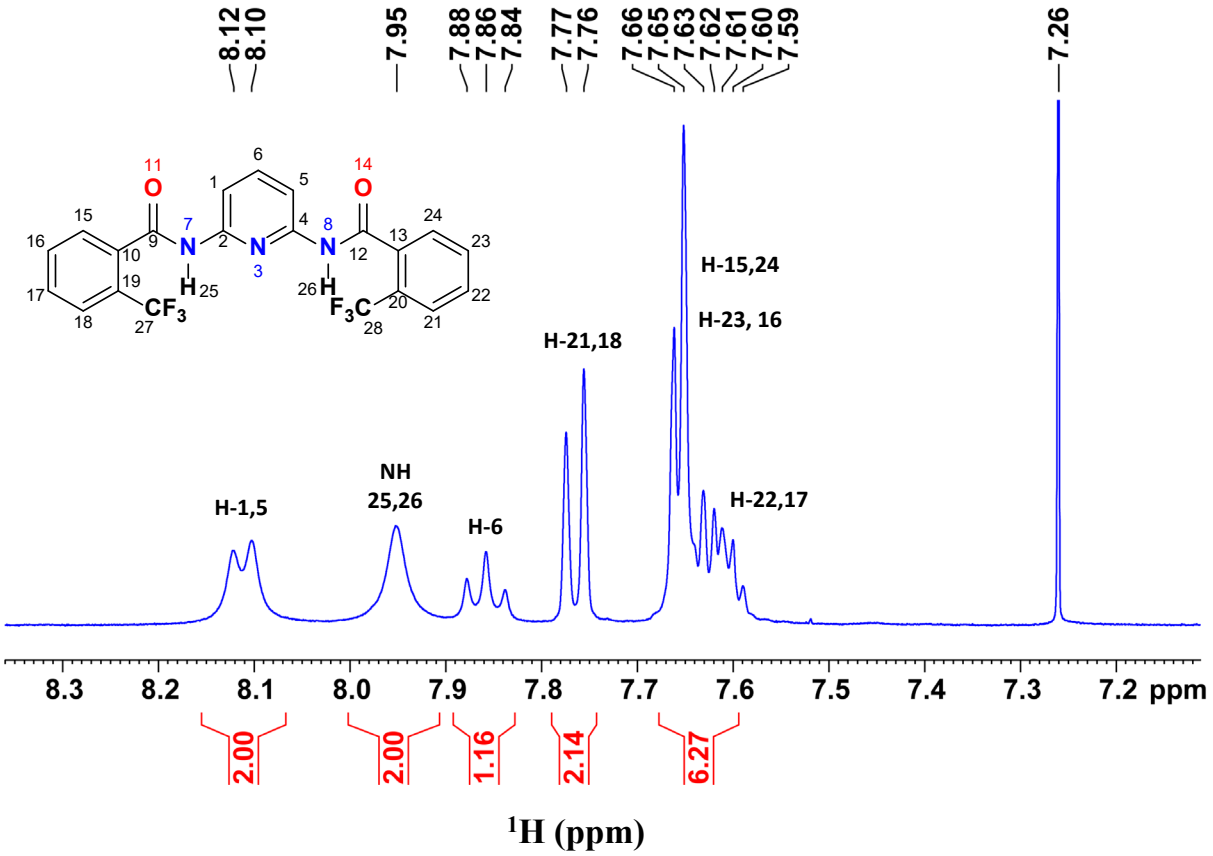

Figure S18: 400 MHz ^{1}H NMR spectrum of A4 molecule in $CDCl_3$ solvent.

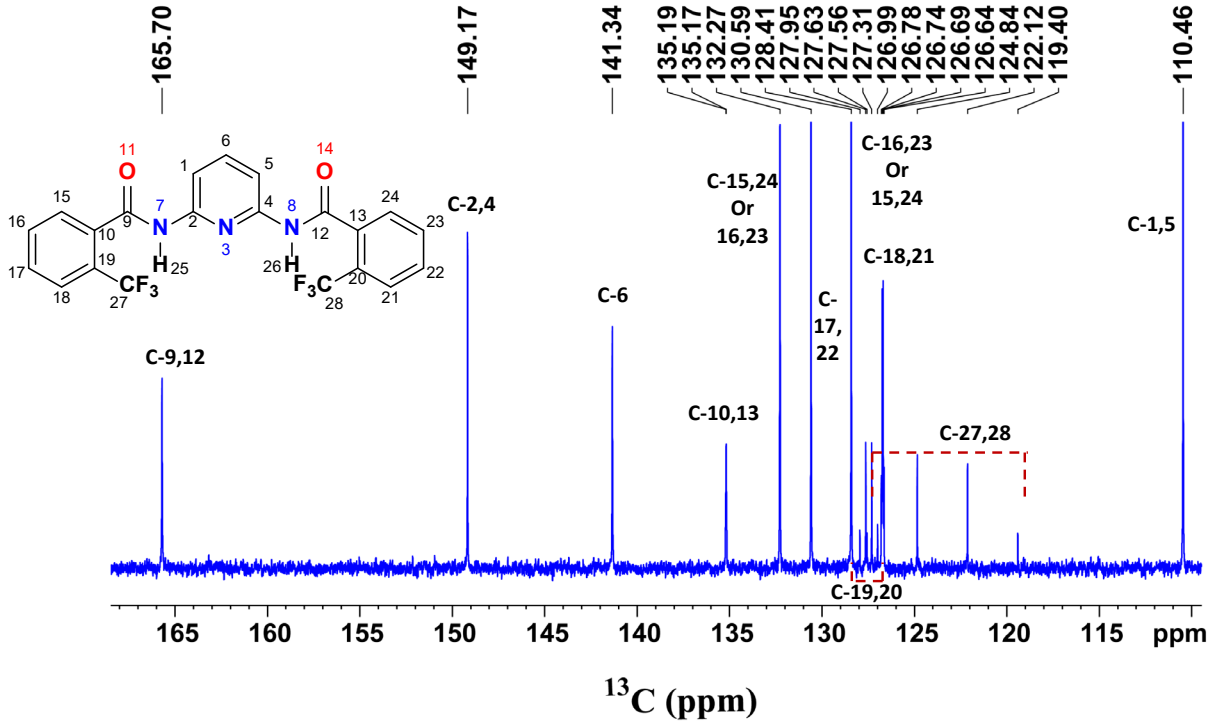

Figure S19: 100 MHz ^{13}C NMR spectrum of A4 molecule in $CDCl_3$ solvent.

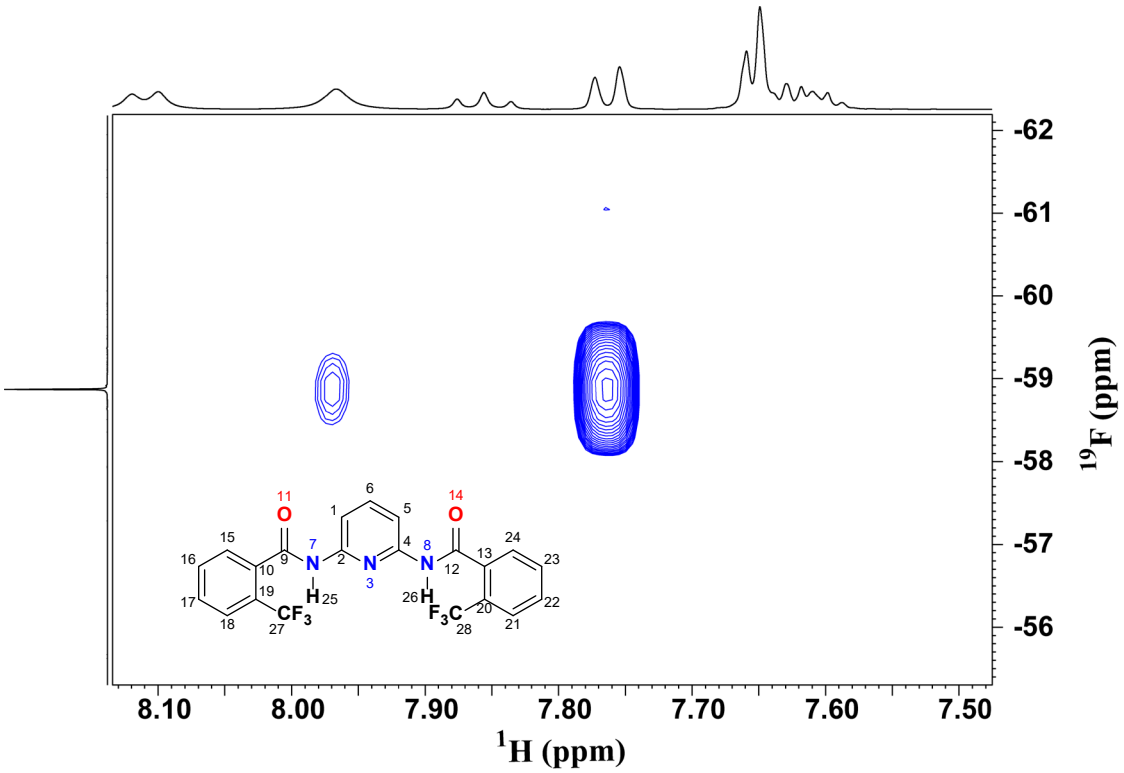

Figure S20: 2D ^{1}H-^{19}F HOESY spectrum of A4 molecule in $CDCl_3$ solvent.

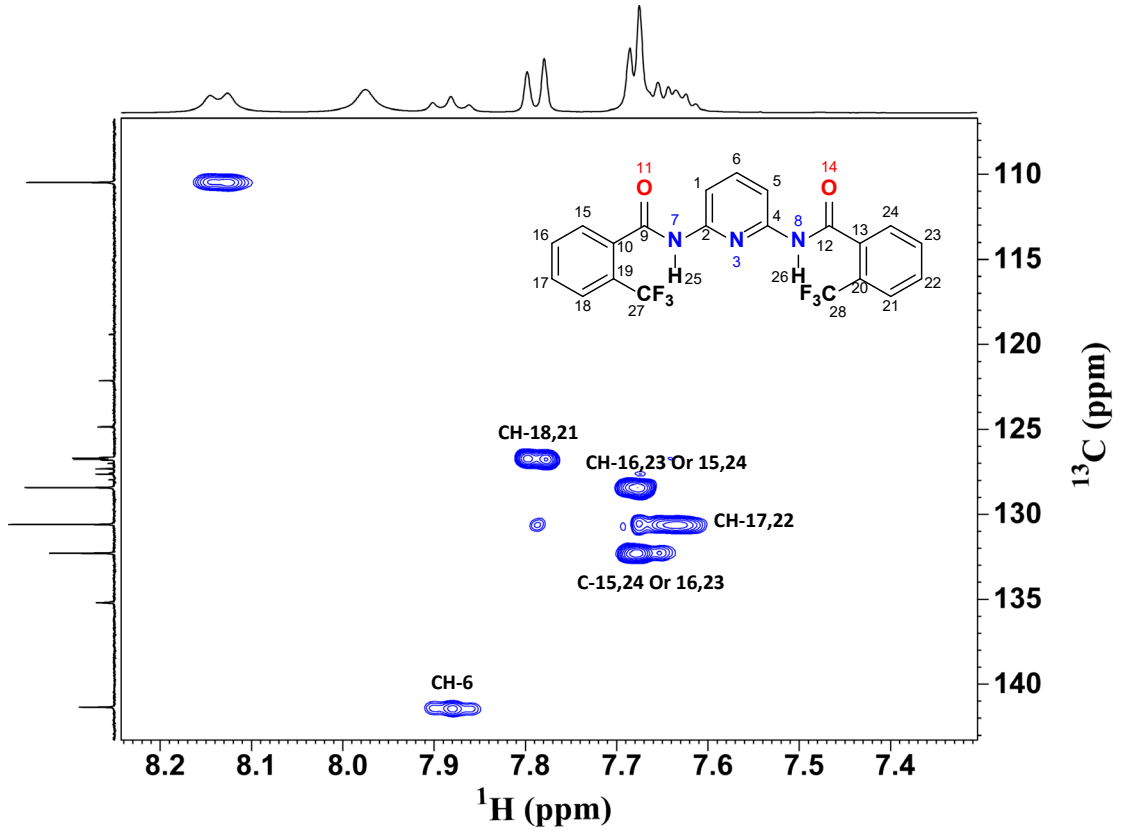

Figure S21: 2D ^{13}C-^{1}H HSQC spectrum of A4 molecule in $CDCl_3$ solvent.

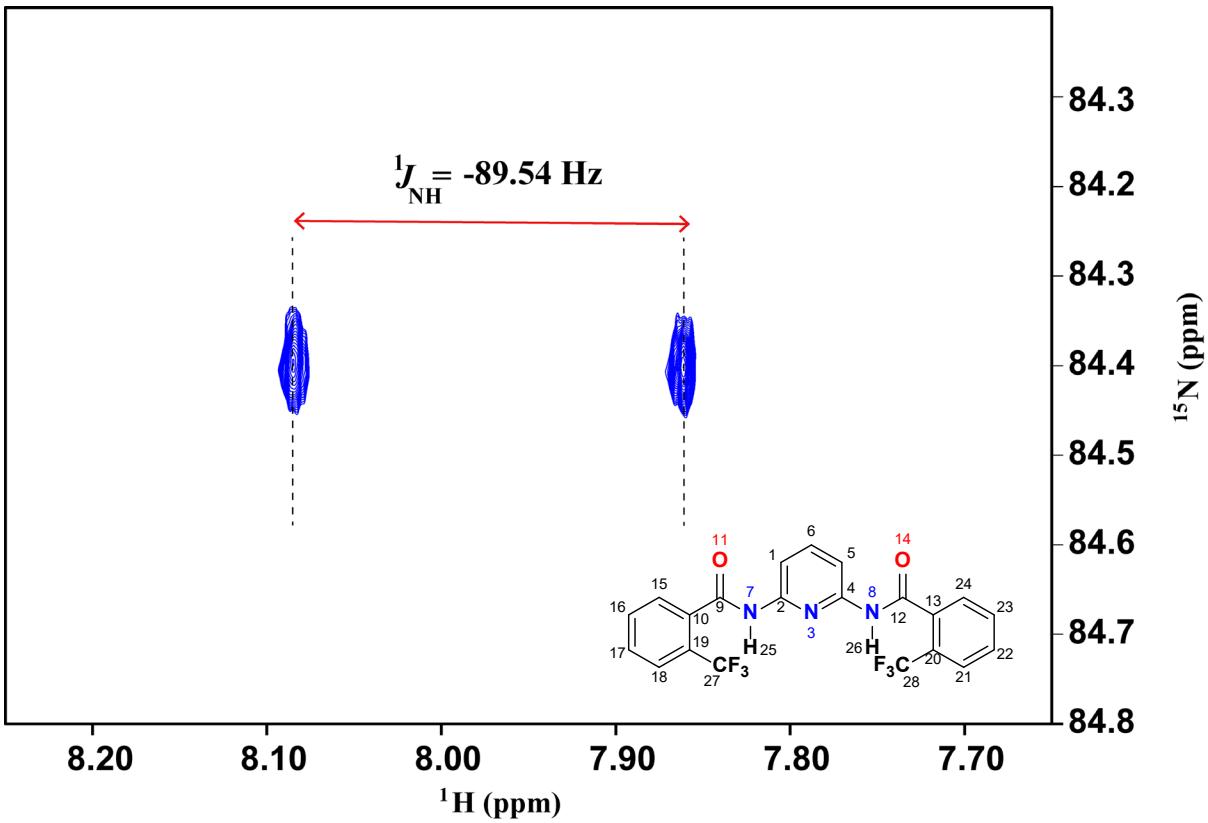

Figure S22: ^{1}H-coupled 2D ^{1}H-^{15}N HSQC spectrum of A4 molecule in $CDCl_3$ solvent.

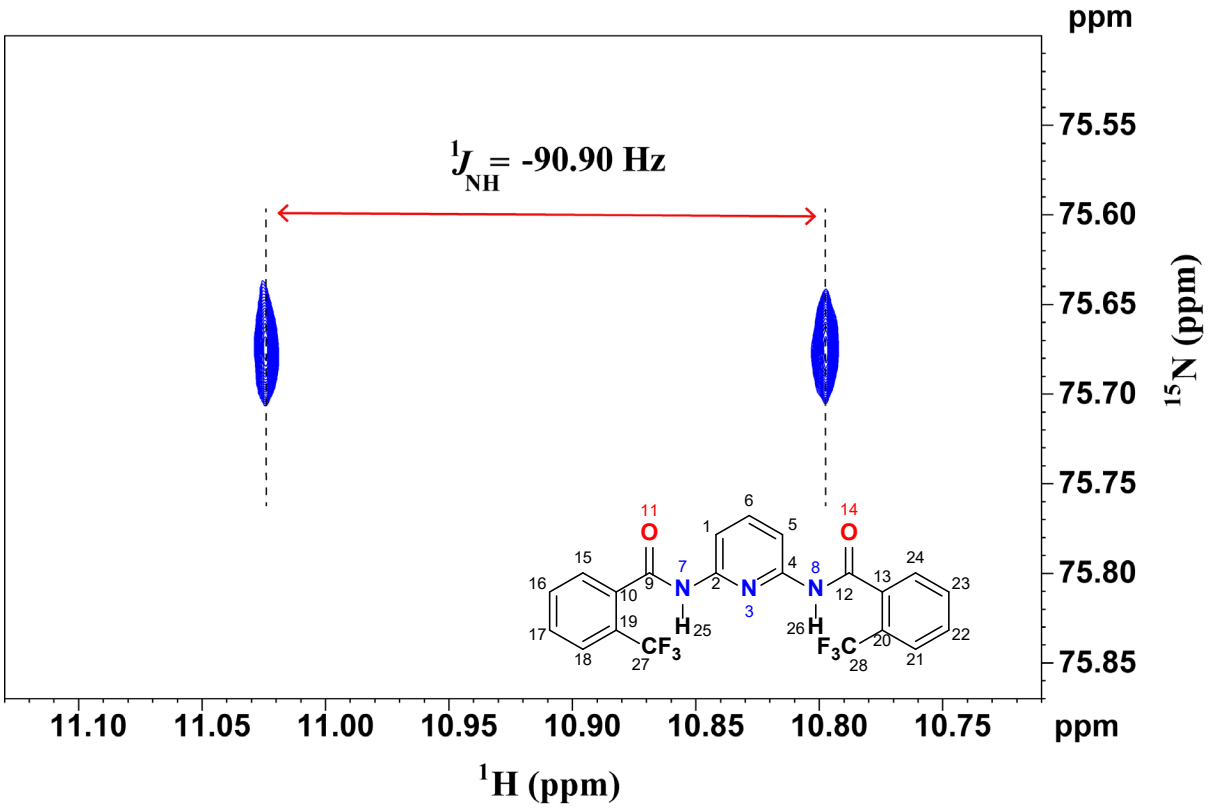

Figure S23: ^{1}H-coupled 2D ^{1}H-^{15}N HSQC spectrum of A4 molecule in DMSO-d_6 solvent.

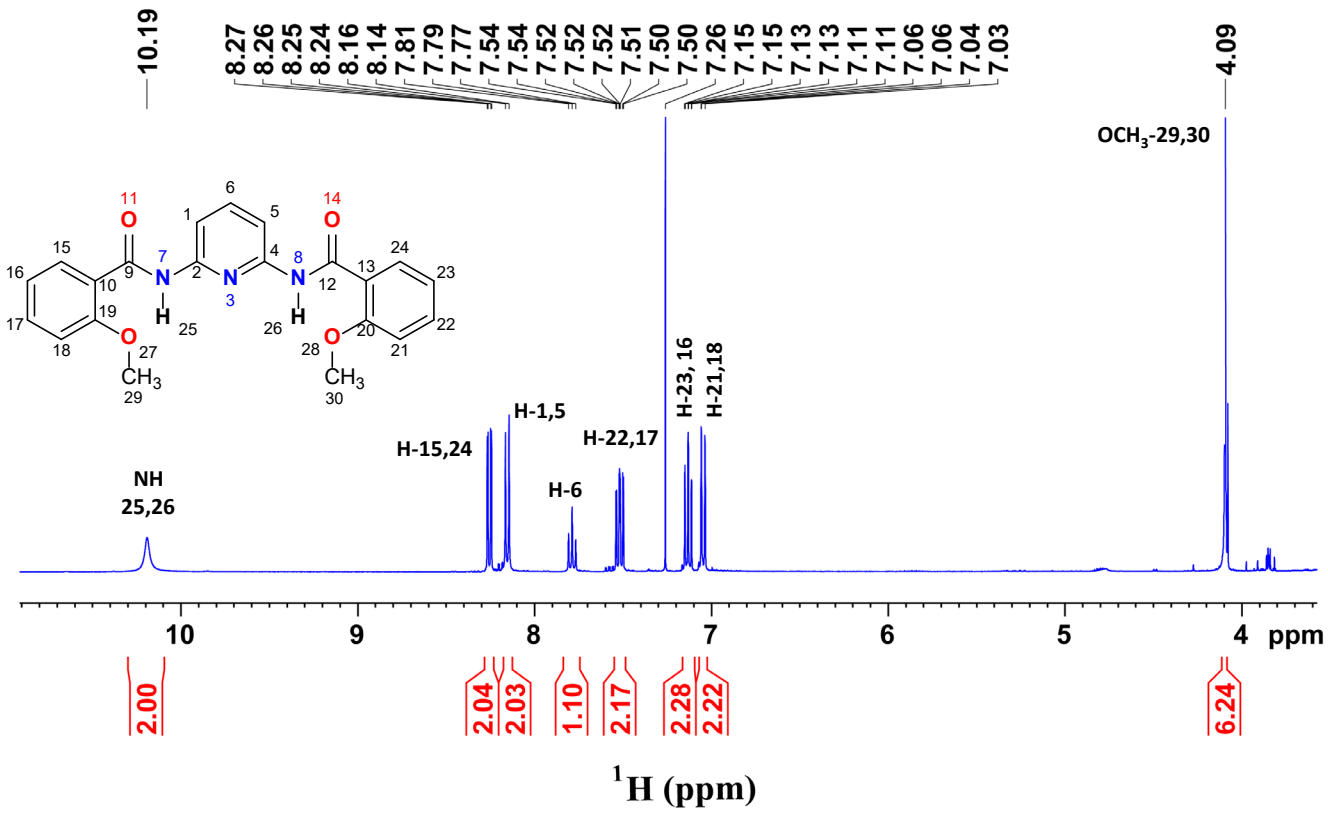

Figure S24: 400 MHz ^{1}H NMR spectrum of A5 molecule in $CDCl_3$ solvent

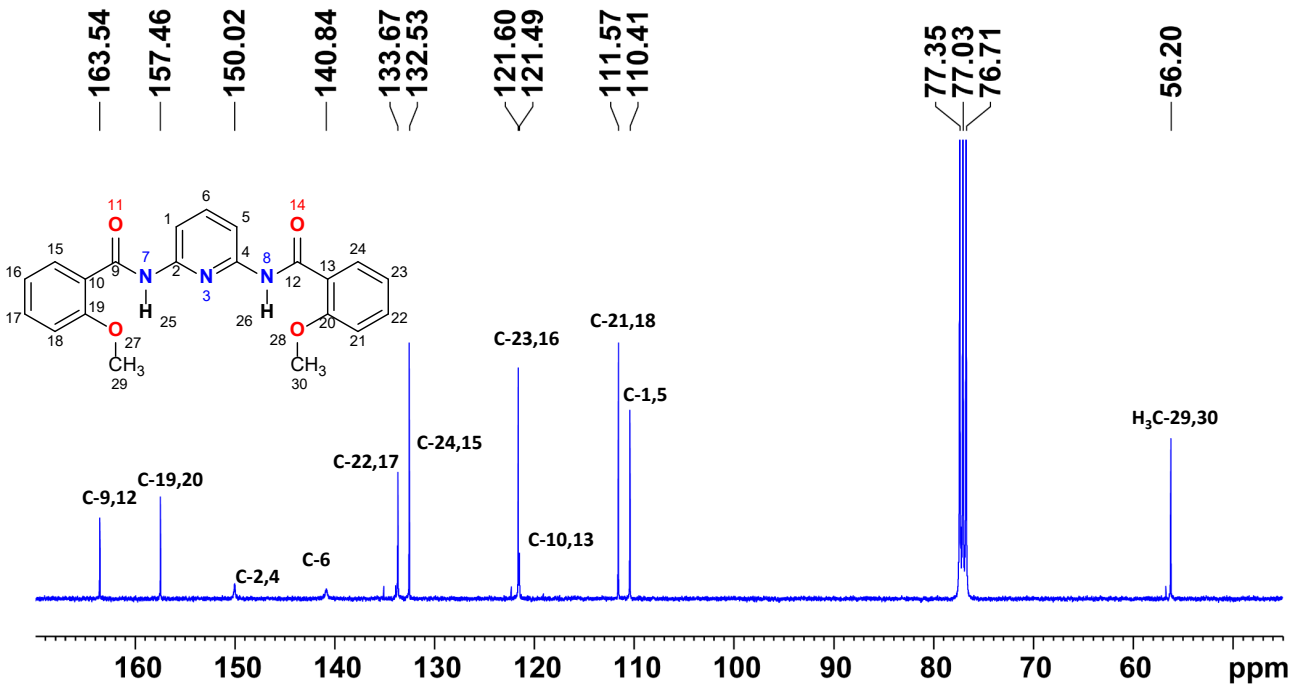

Figure S25:100 MHz ^{13}C NMR spectrum of A5 molecule in $CDCl_3$ solvent

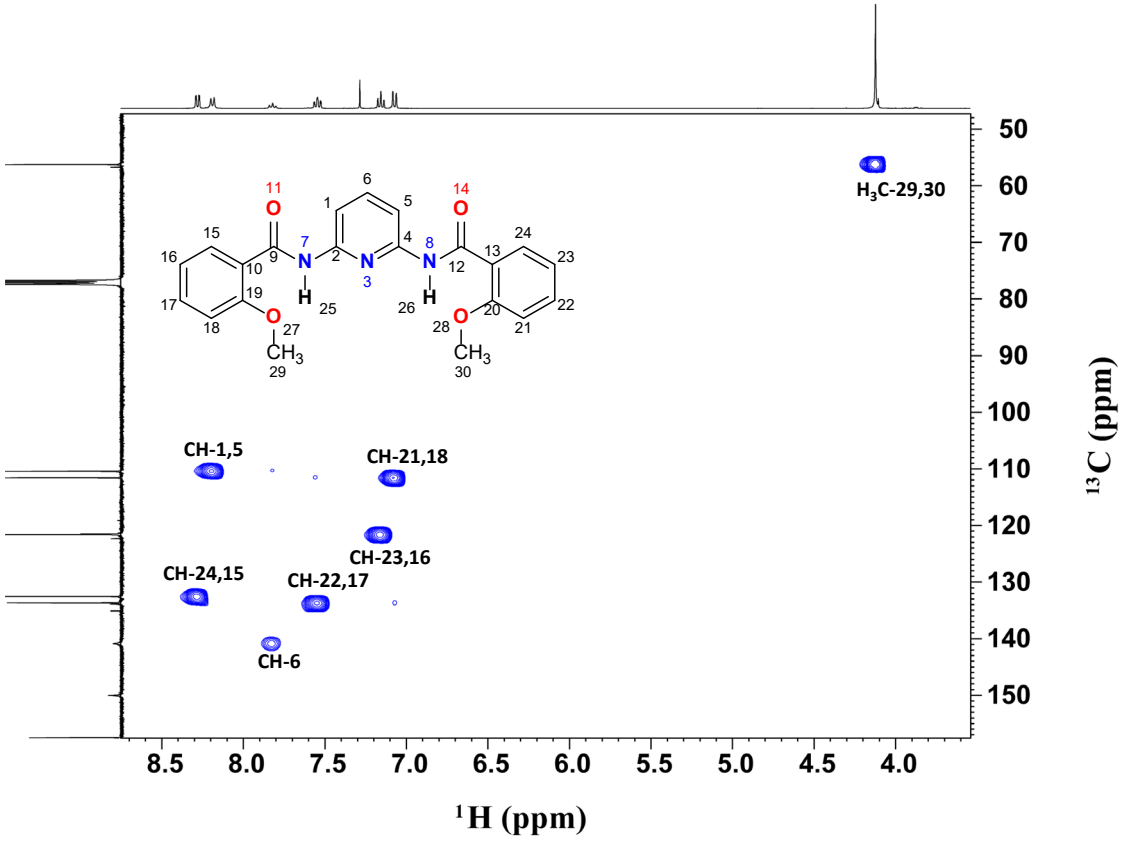

Figure S26: 2D ^{13}C-^{1}H HSQC spectrum of A5 molecule in $CDCl_3$ solvent

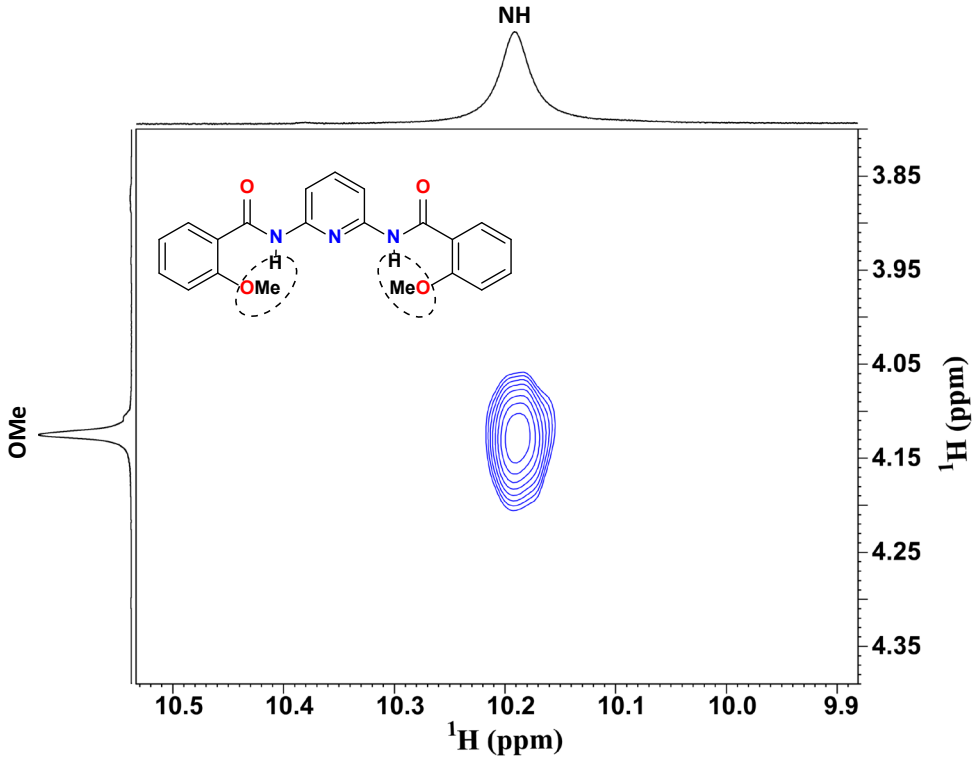

Figure S27: 2D NOESY Spectrum of A5 molecule at 400 MHz in $CDCl_3$ solvent

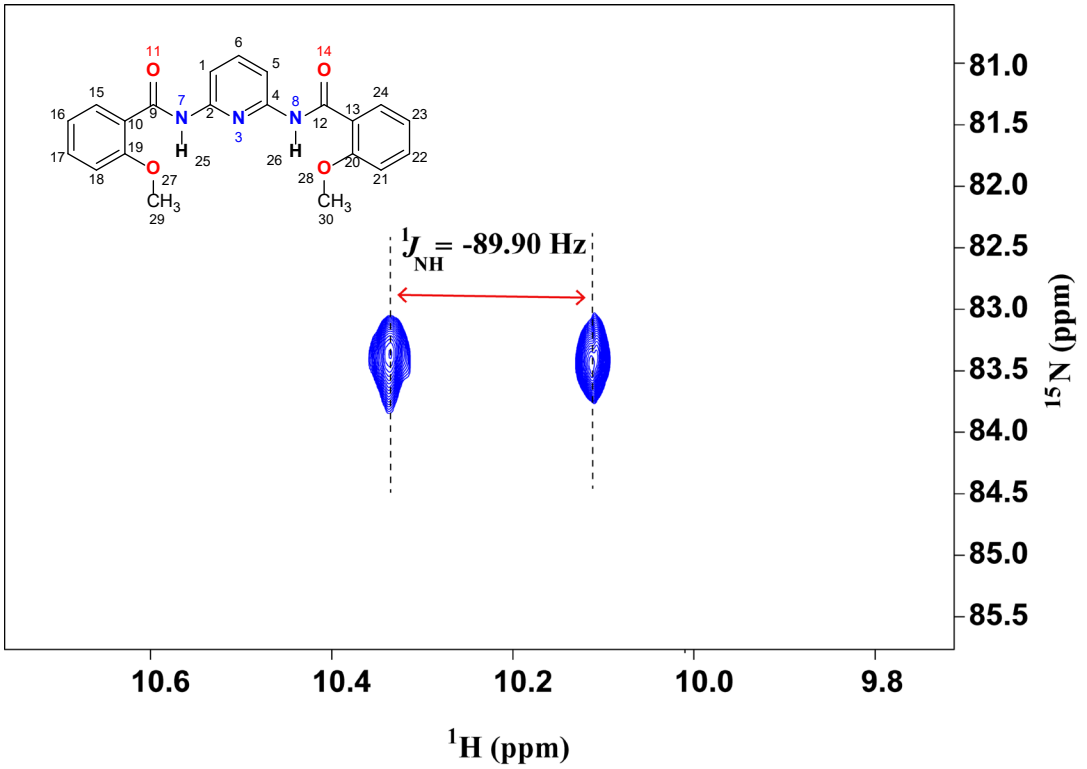

Figure S28: ^{1}H-coupled 2D ^{1}H-^{15}N HSQC spectrum of A5 molecule measured in $CDCl_3$ solvent.

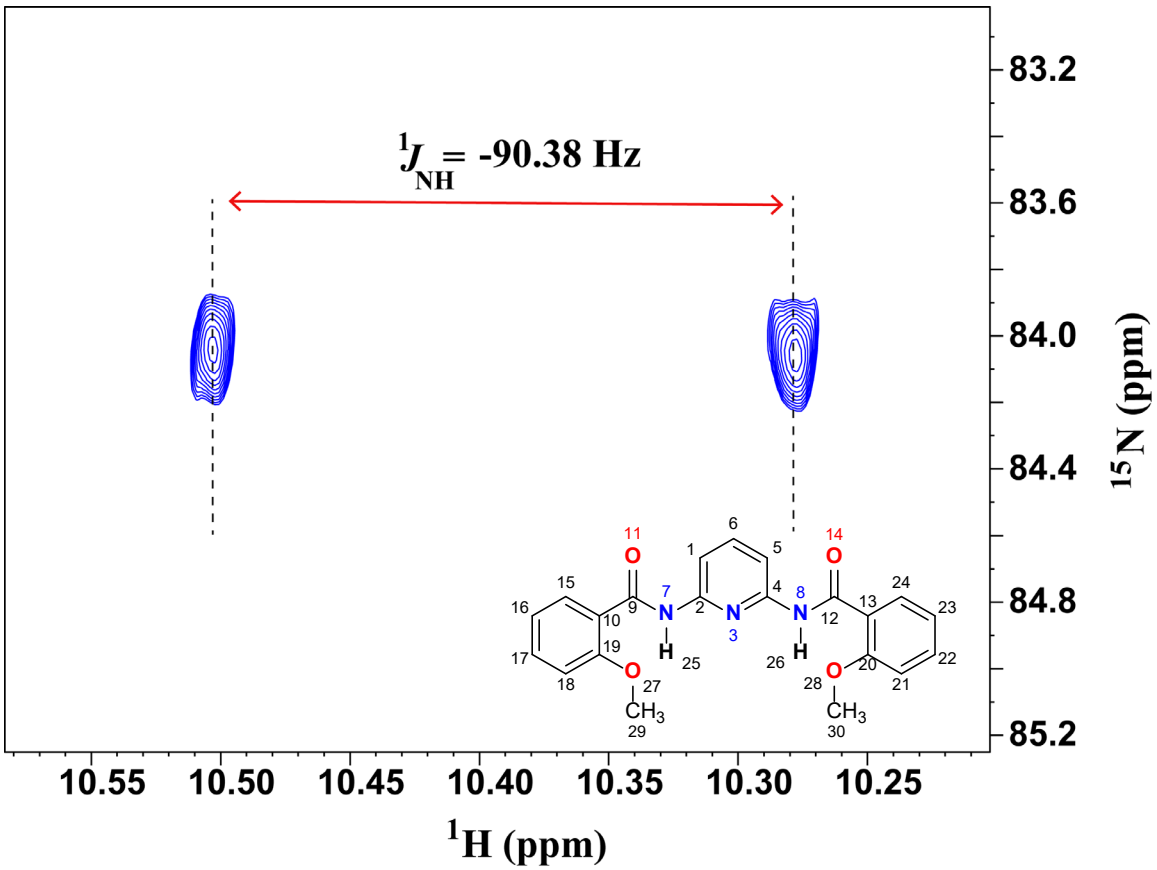

Figure S29: ^{1}H-coupled 2D ^{1}H-^{15}N HSQC spectrum of A5 molecule in DMSO-d_6 solvent.

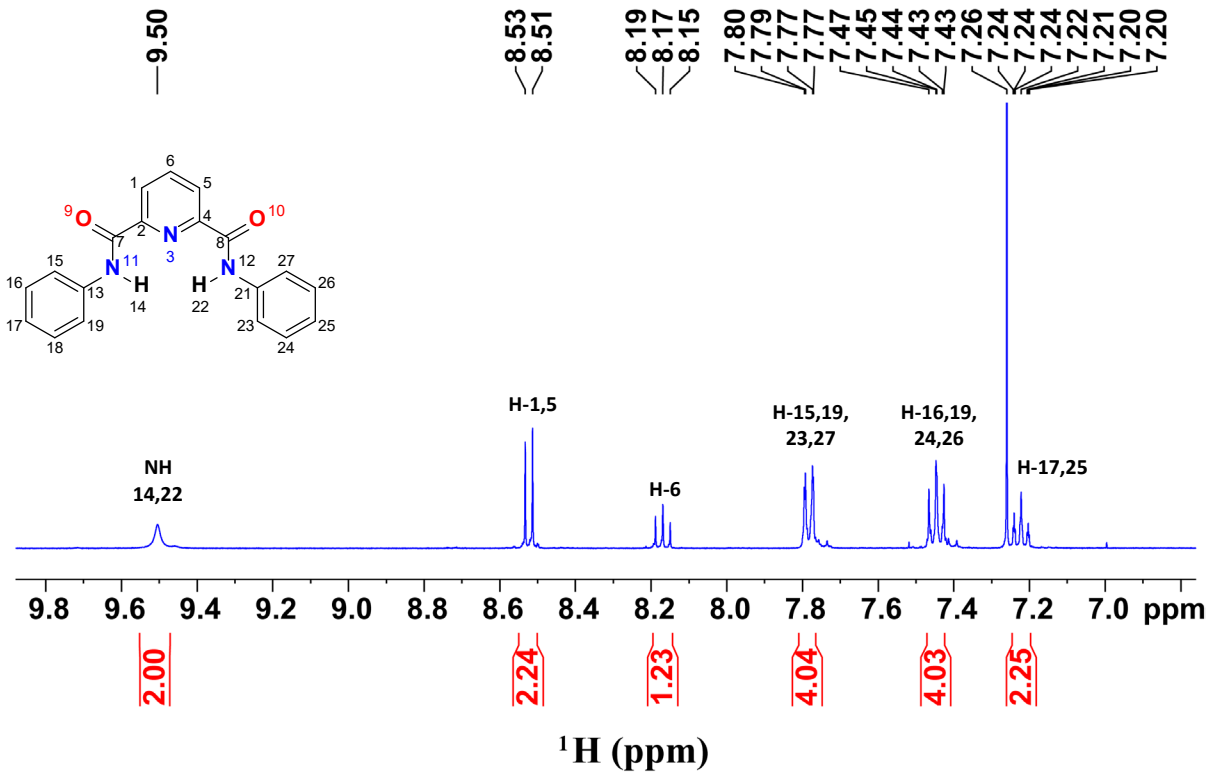

Figure S30: 400 MHz ^{1}H NMR spectrum of B1 molecule in $CDCl_3$ solvent.

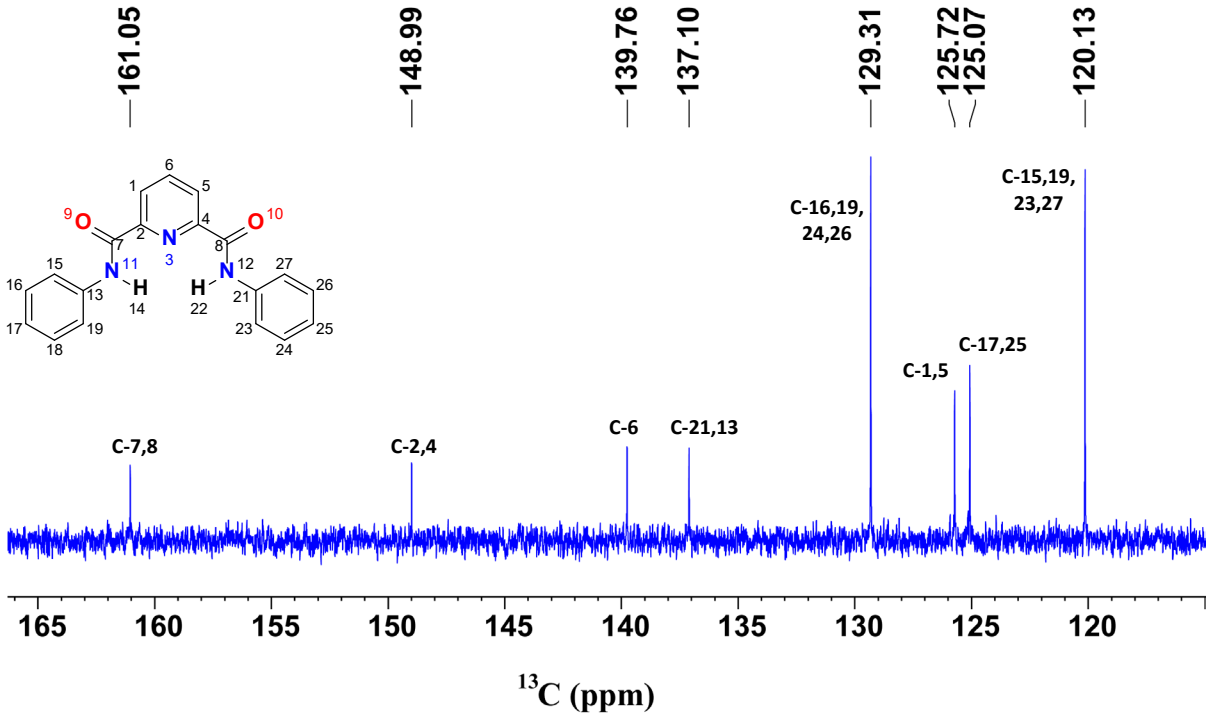

Figure S31:100 MHz ^{13}C NMR spectrum of B1 molecule in $CDCl_3$ solvent.

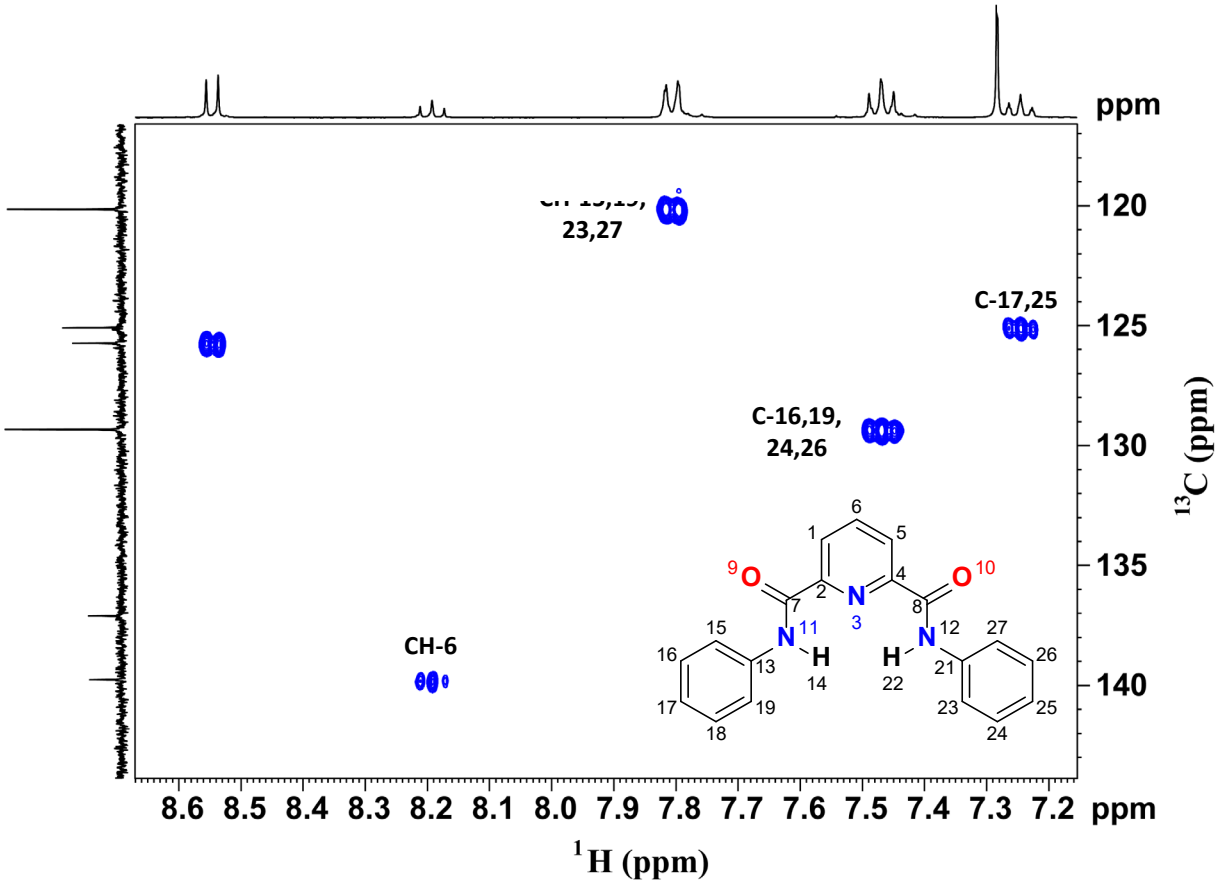

Figure S32: 2D ^{13}C-^{1}H HSQC spectrum of B1 molecule in $CDCl_3$ solvent

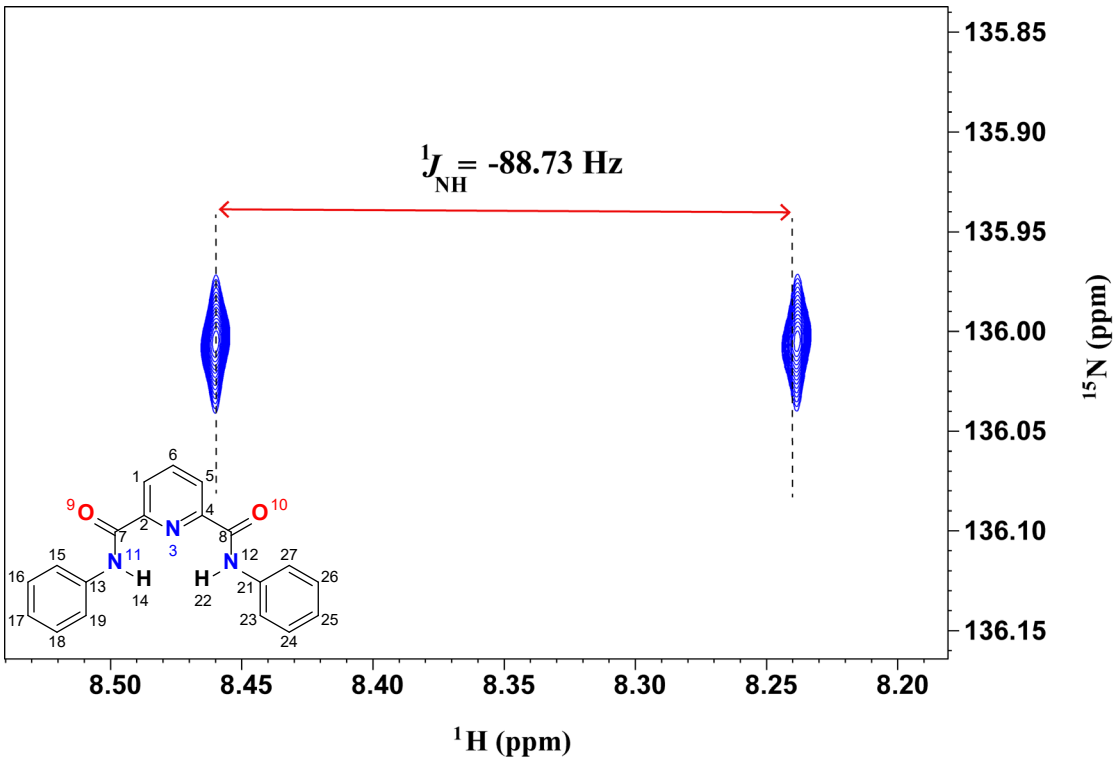

Figure S33: ^{1}H-coupled 2D ^{1}H-^{15}N HSQC spectrum of B1 molecule in $CDCl_3$ solvent

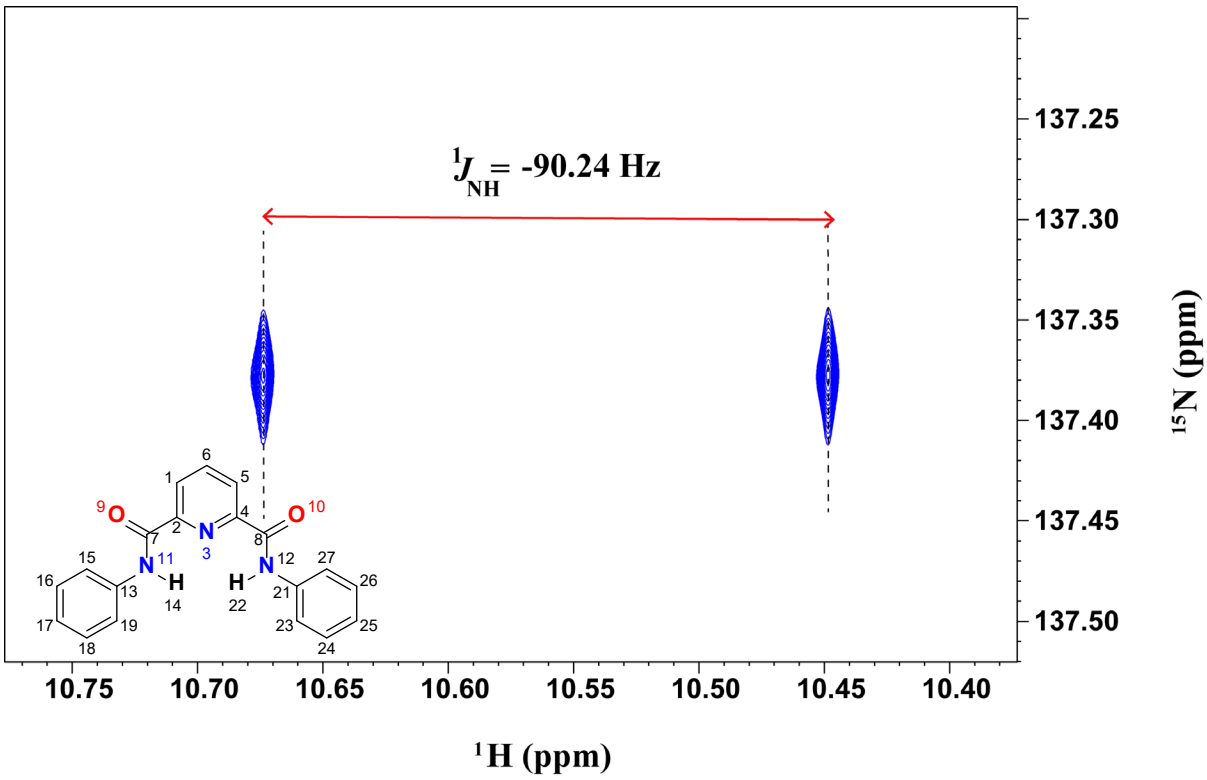

Figure S34: ^{1}H-coupled 2D ^{1}H-^{15}N HSQC spectrum of B1 molecule measured at 400 MHz in DMSO-d_6 solvent

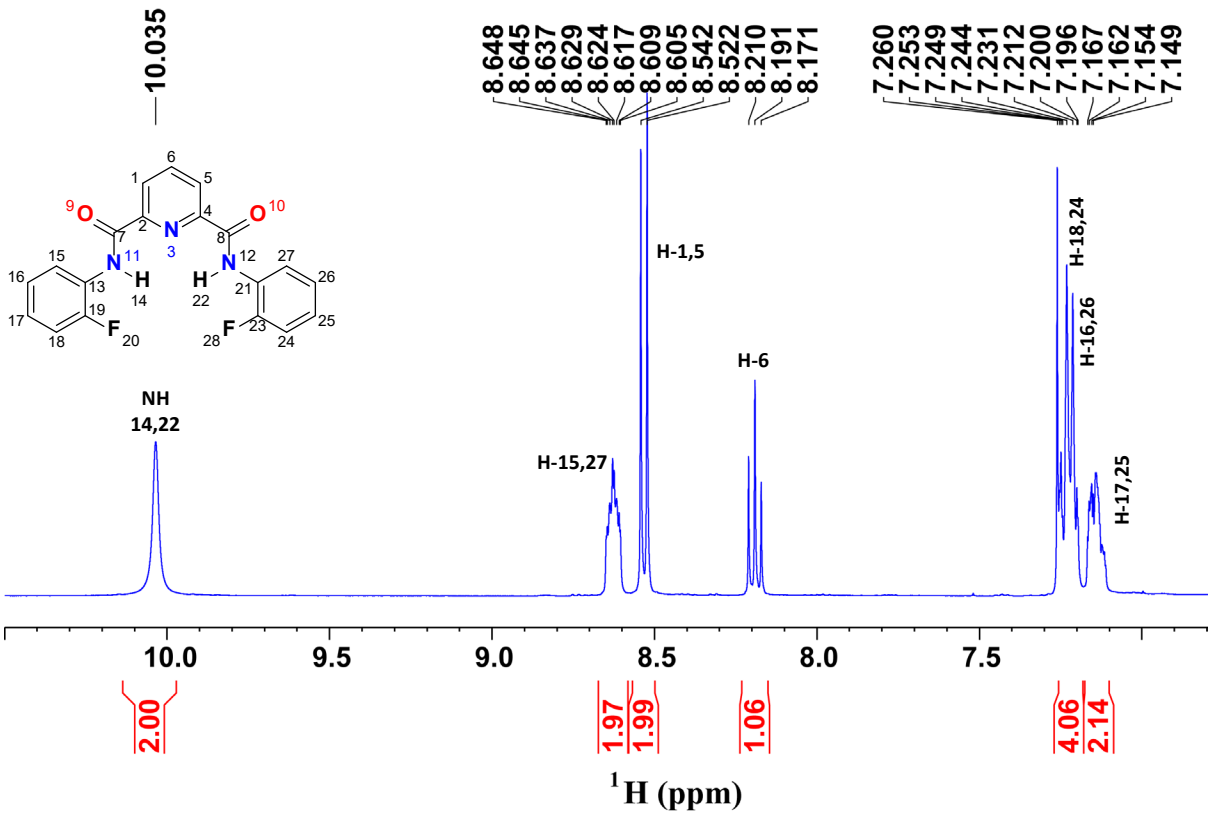

Figure S35: 400 MHz ^{1}H NMR spectrum of B2 molecule in $CDCl_3$ solvent.

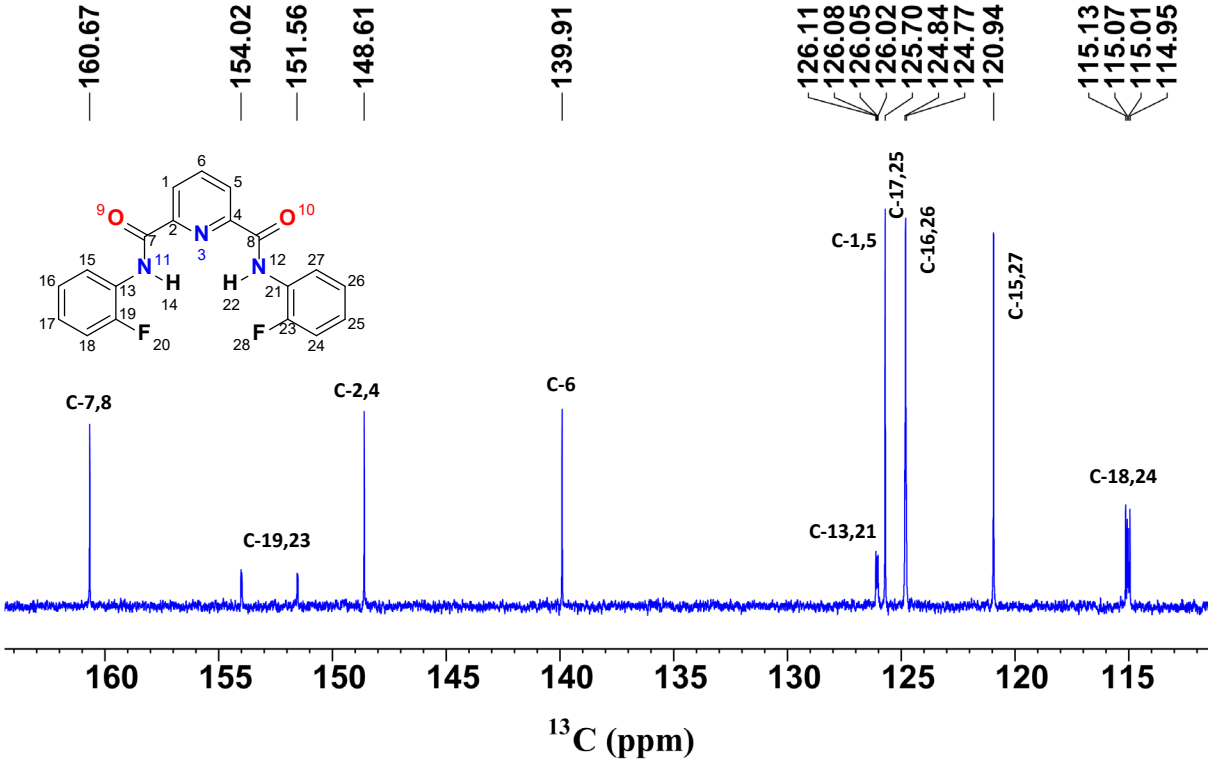

Figure S36: 100 MHz ^{13}C NMR spectrum of B2 molecule in $CDCl_3$ solvent.

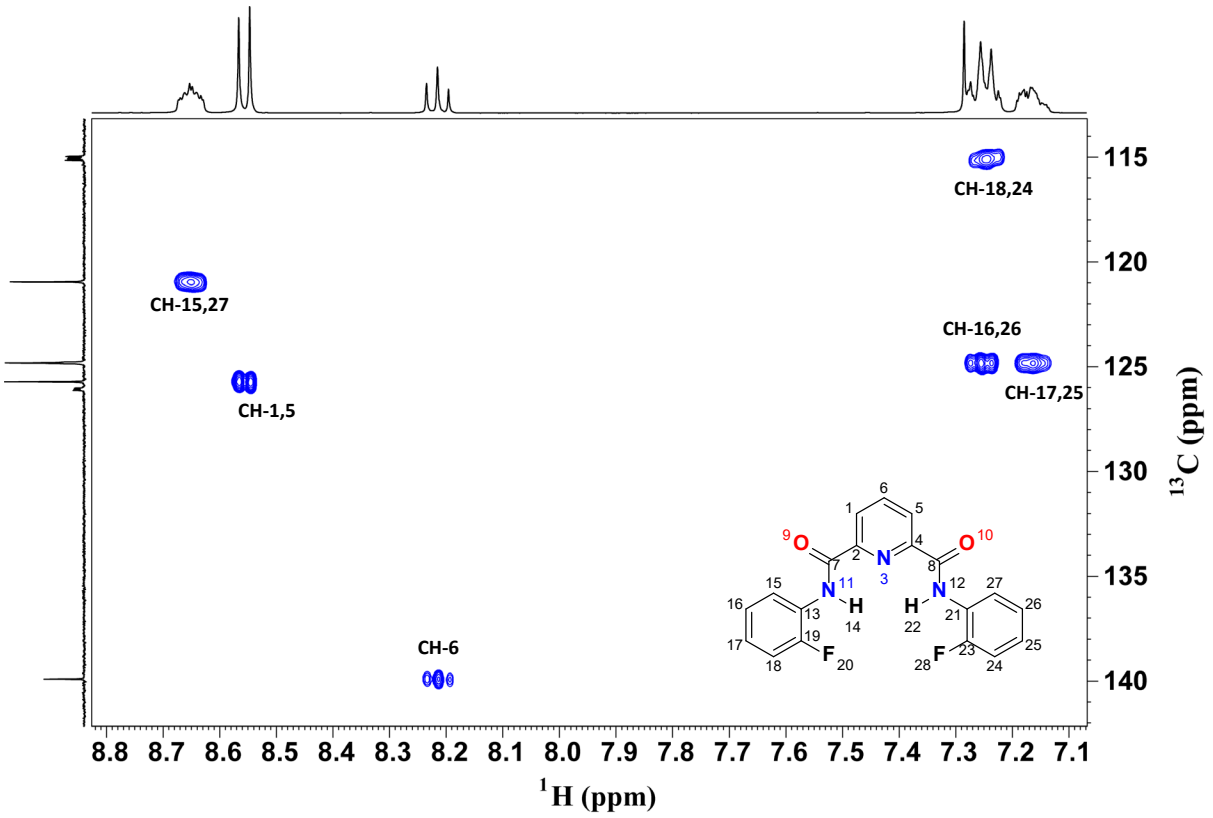

Figure S37: 2D ^{13}C-^{1}H HSQC spectrum of B2 molecule in $CDCl_3$ solvent

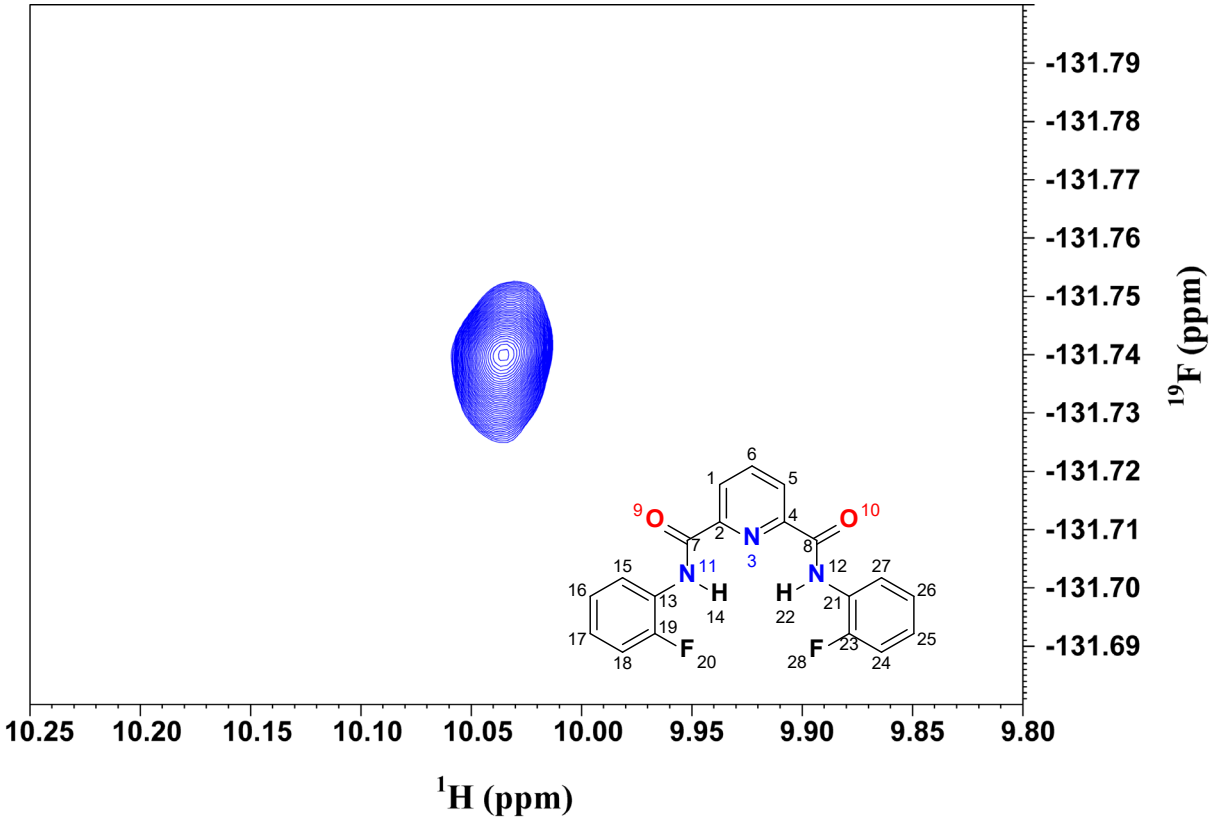

Figure S38: 2D ^{1}H-^{19}F HOESY spectrum of B2 molecule in $CDCl_3$ solvent.

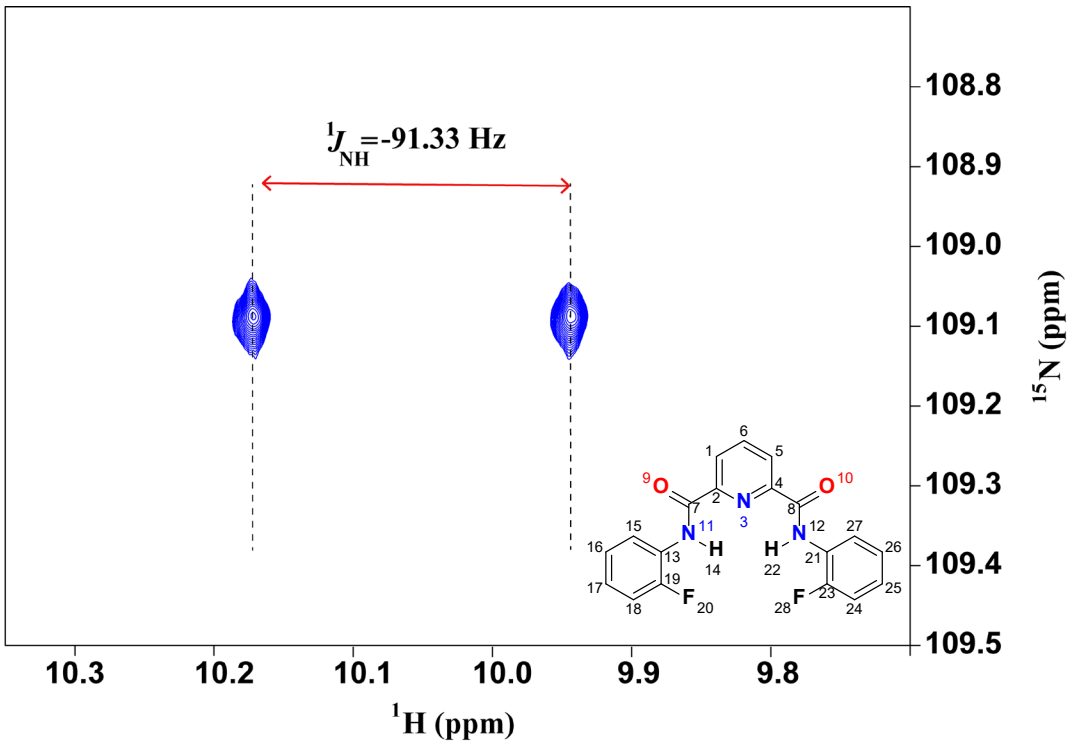

Figure S39: ^{1}H-coupled 2D ^{1}H-^{15}N HSQC spectrum of B2 molecule in $CDCl_3$ solvent

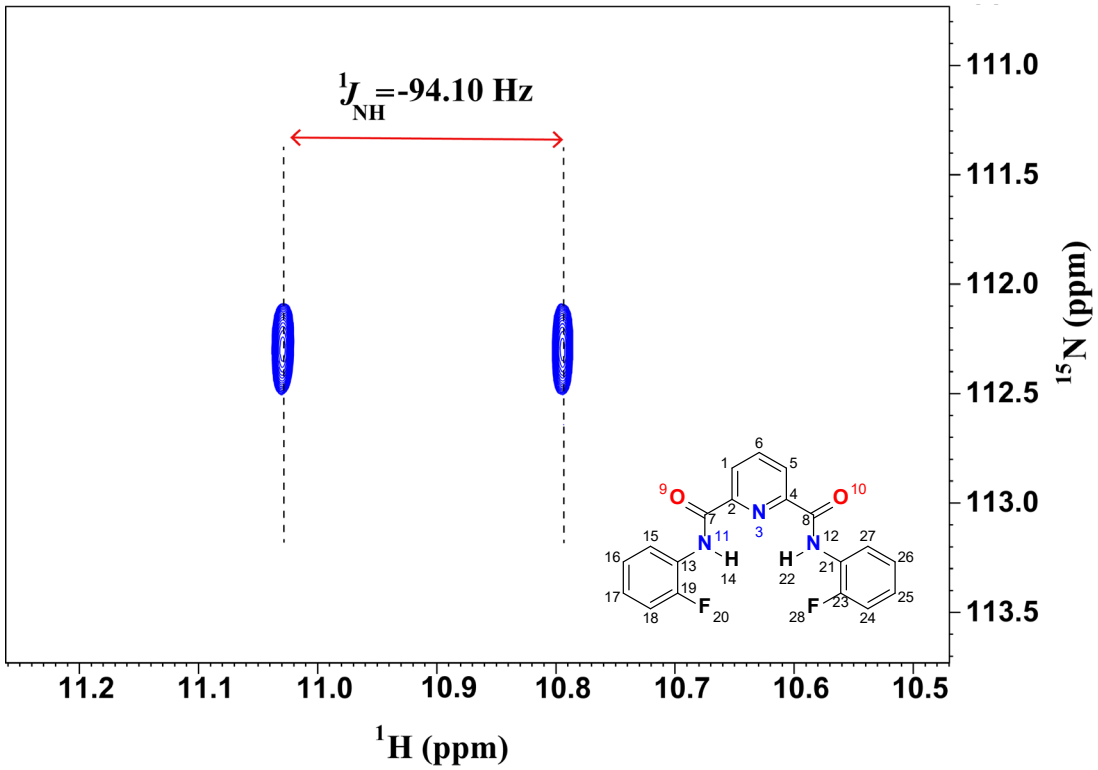

Figure S40: ^{1}H-coupled 2D ^{1}H-^{15}N HSQC spectrum of B2 molecule in DMSO-d_6 solvent

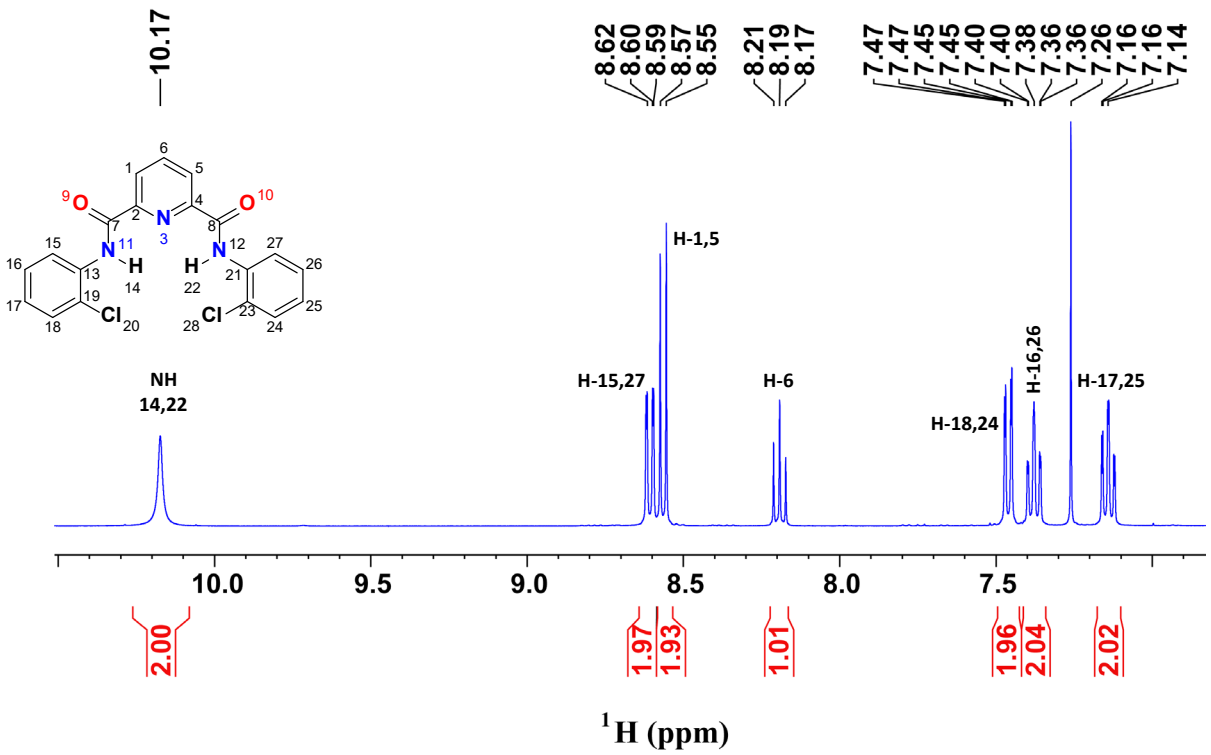

Figure S41: 400 MHz ^{1}H NMR spectrum of B3 molecule in $CDCl_3$ solvent.

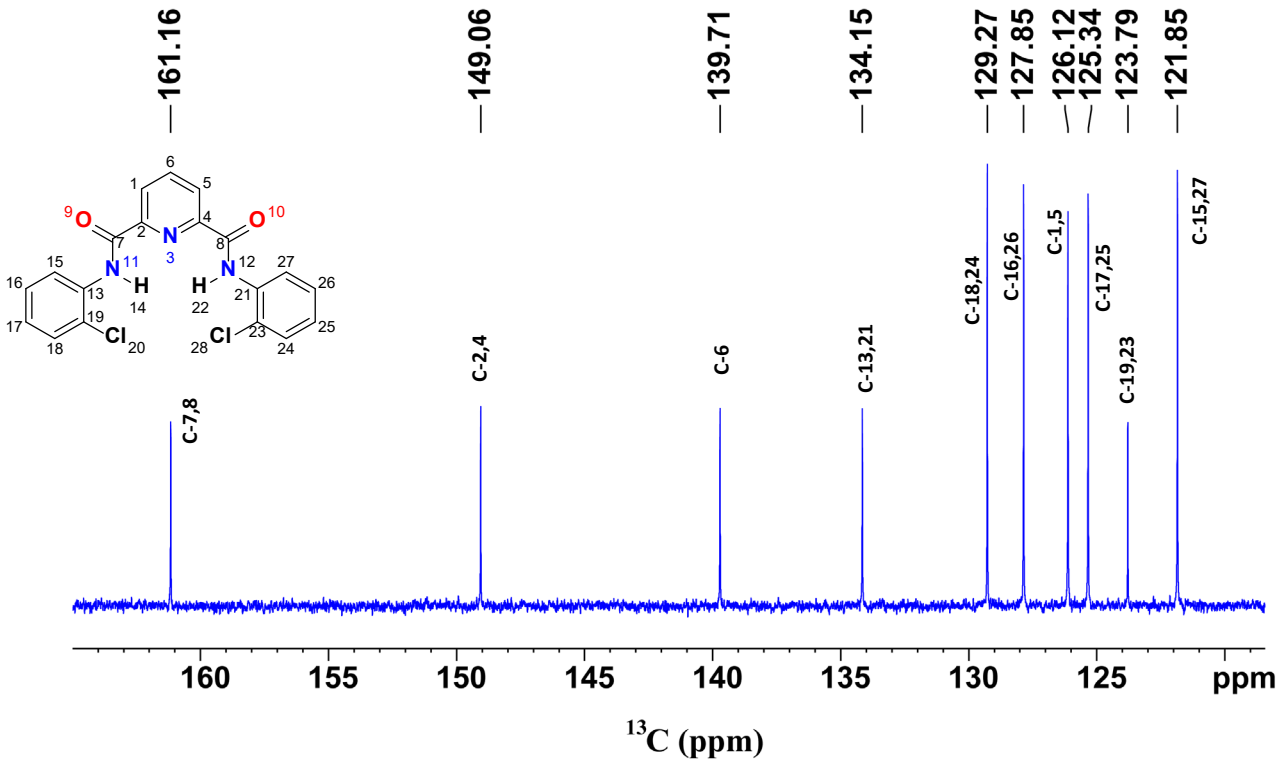

Figure S42: 100 MHz ^{13}C NMR spectrum of B3 molecule in $CDCl_3$ solvent.

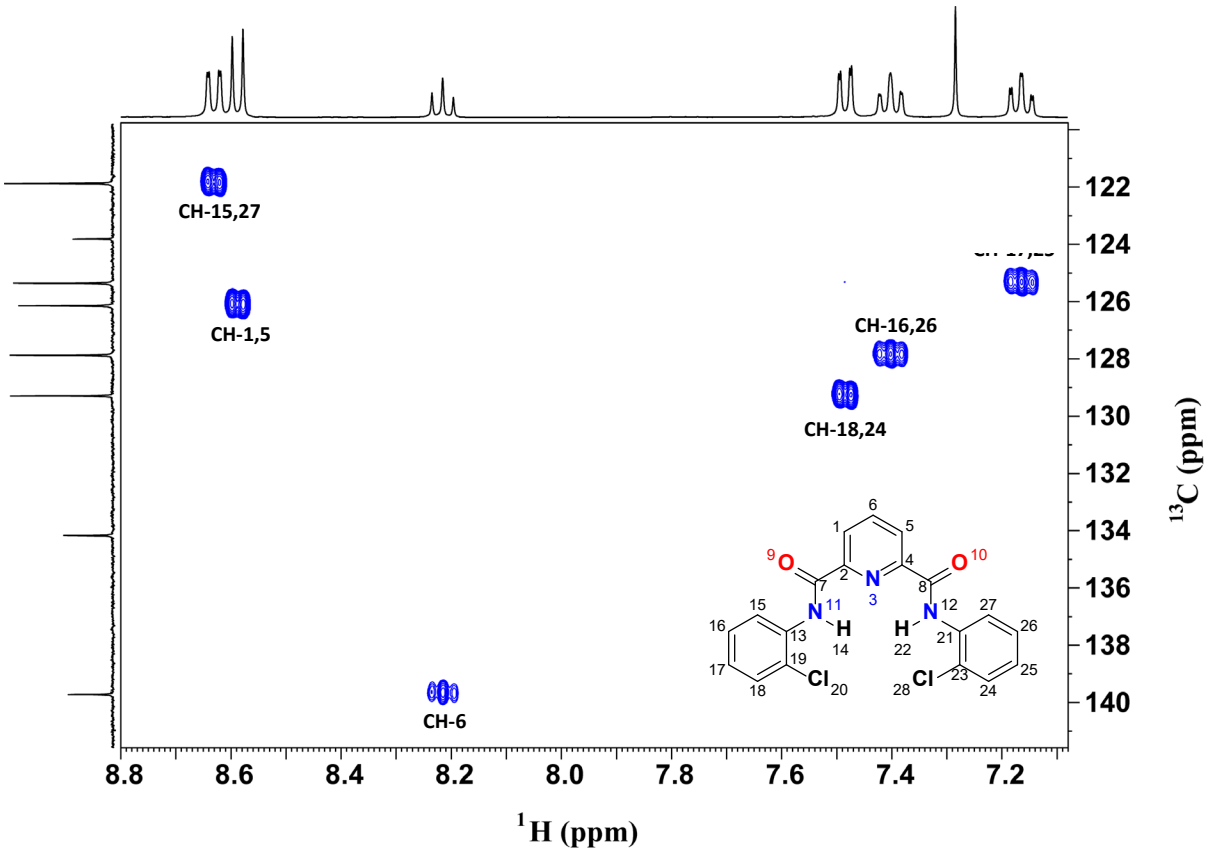

Figure S43:2D ^{13}C-^{1}H HSQC spectrum of B3 molecule in $CDCl_3$ solvent

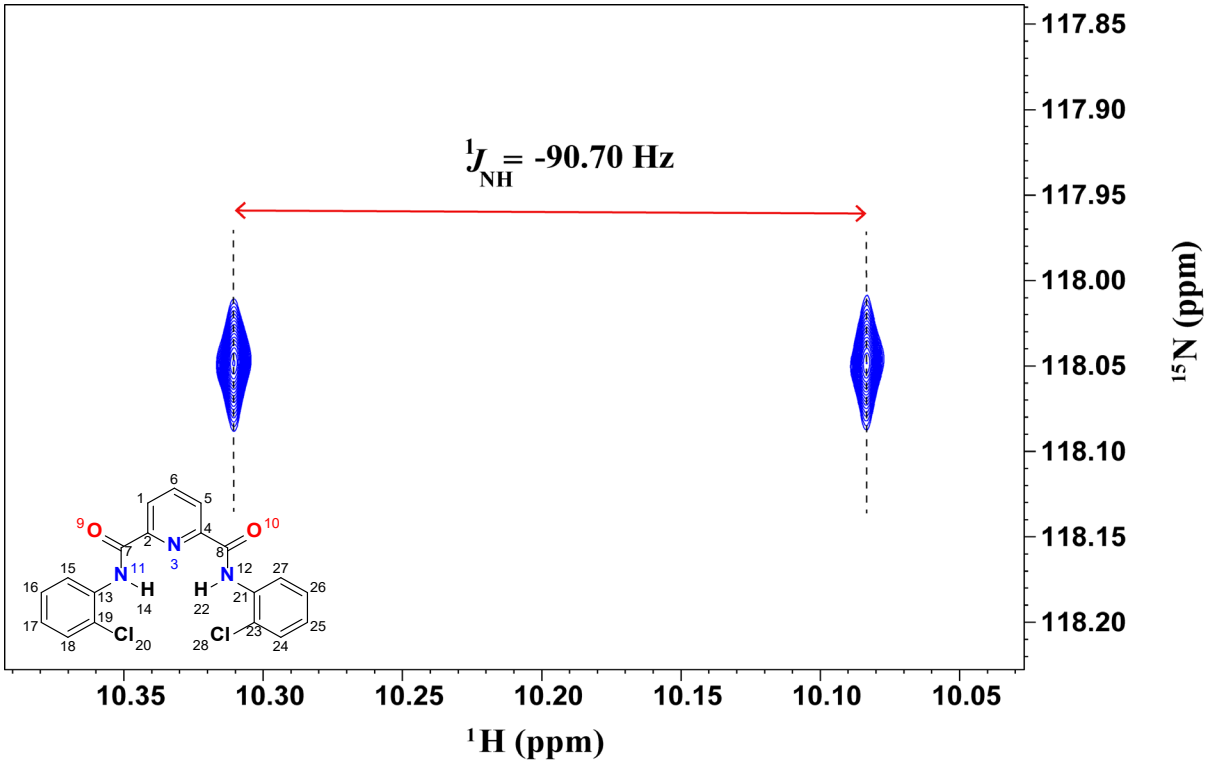

Figure S44: ^{1}H-coupled 2D ^{1}H-^{15}N HSQC spectrum of B3 molecule in $CDCl_3$ solvent

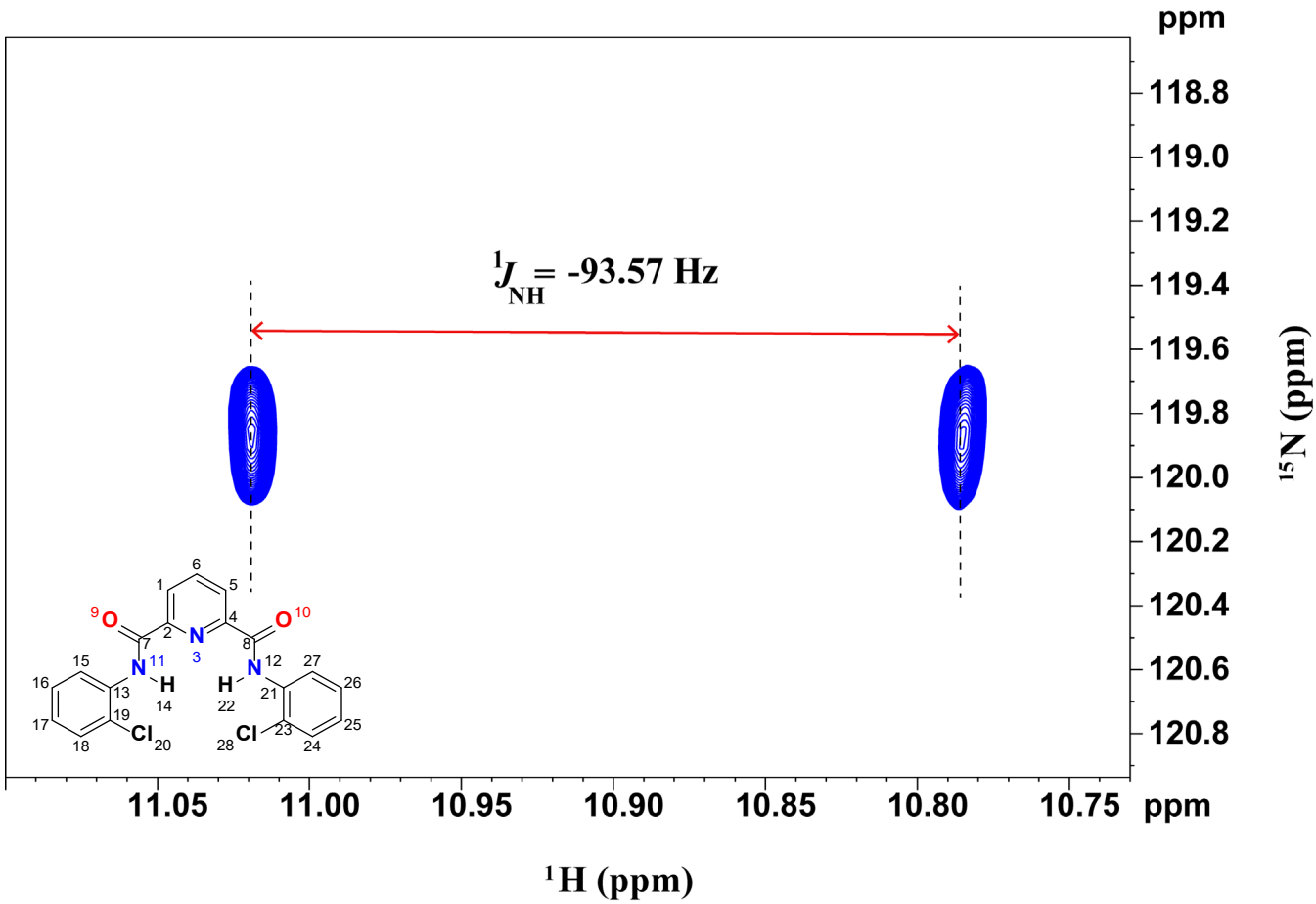

Figure S45: ^{1}H-coupled 2D ^{1}H-^{15}N HSQC spectrum of B3 molecule in DMSO-d_6 solvent

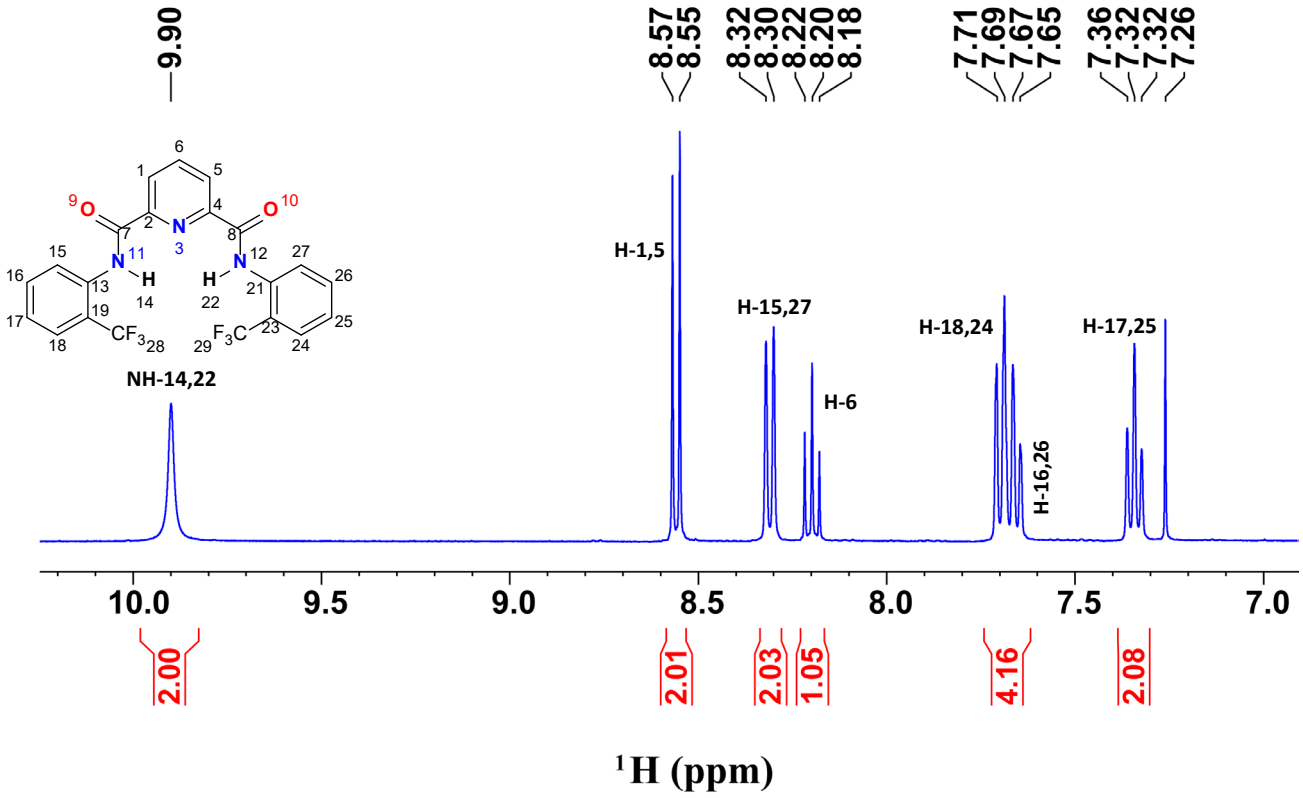

Figure S46: 400 MHz ^{1}H NMR spectrum of B4 molecule in $CDCl_3$ solvent

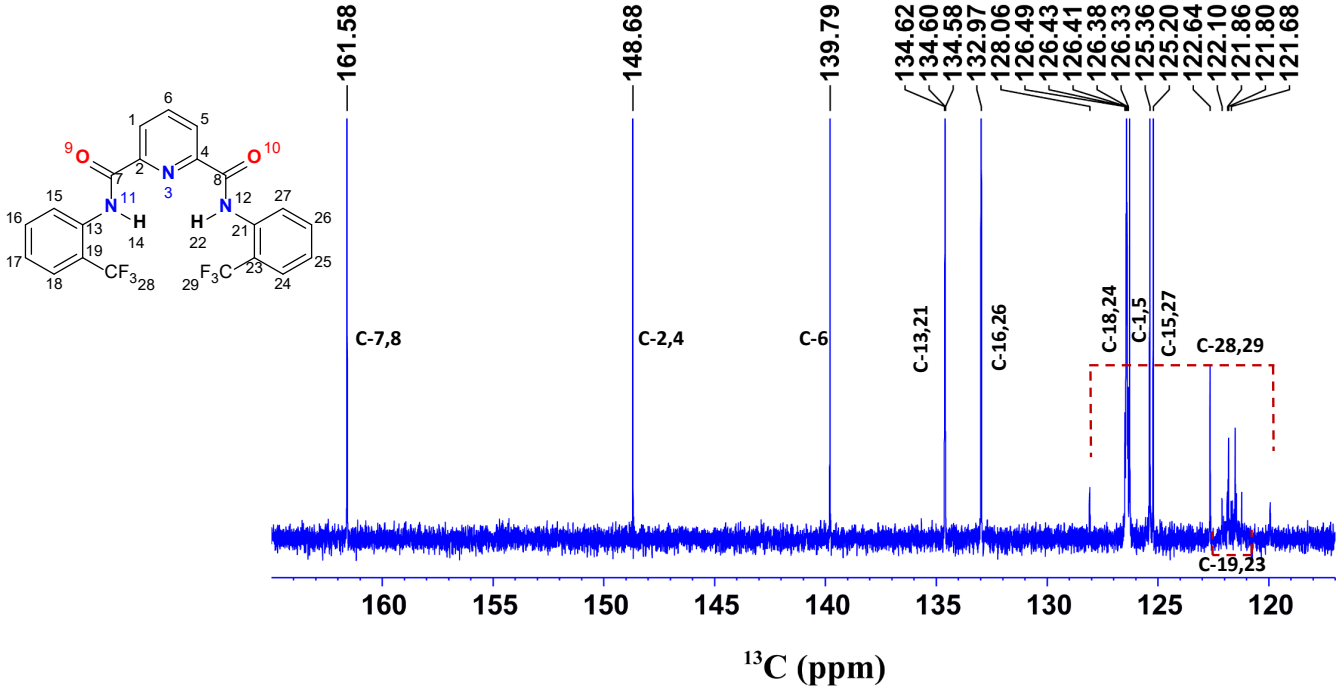

Figure S47: 100 MHz ^{13}C NMR spectrum of B4 molecule in $CDCl_3$ solvent.

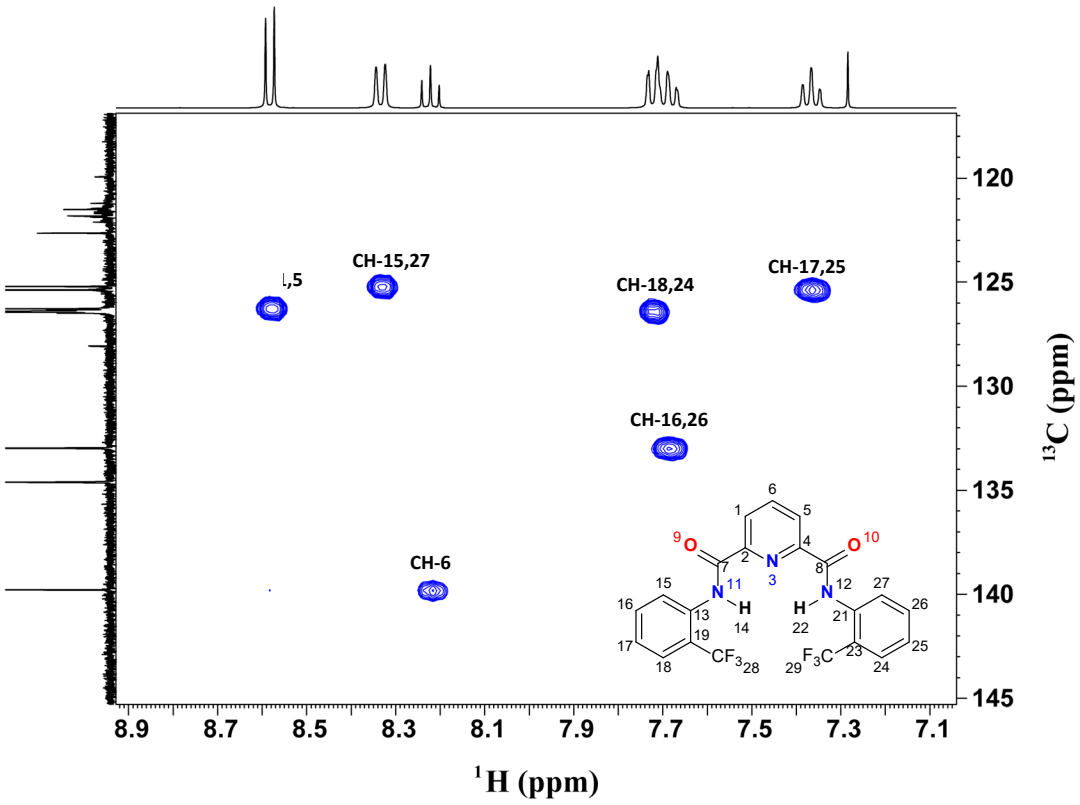

Figure S48: 2D ^{13}C-^{1}H HSQC spectrum of B4 molecule in $CDCl_3$ solvent

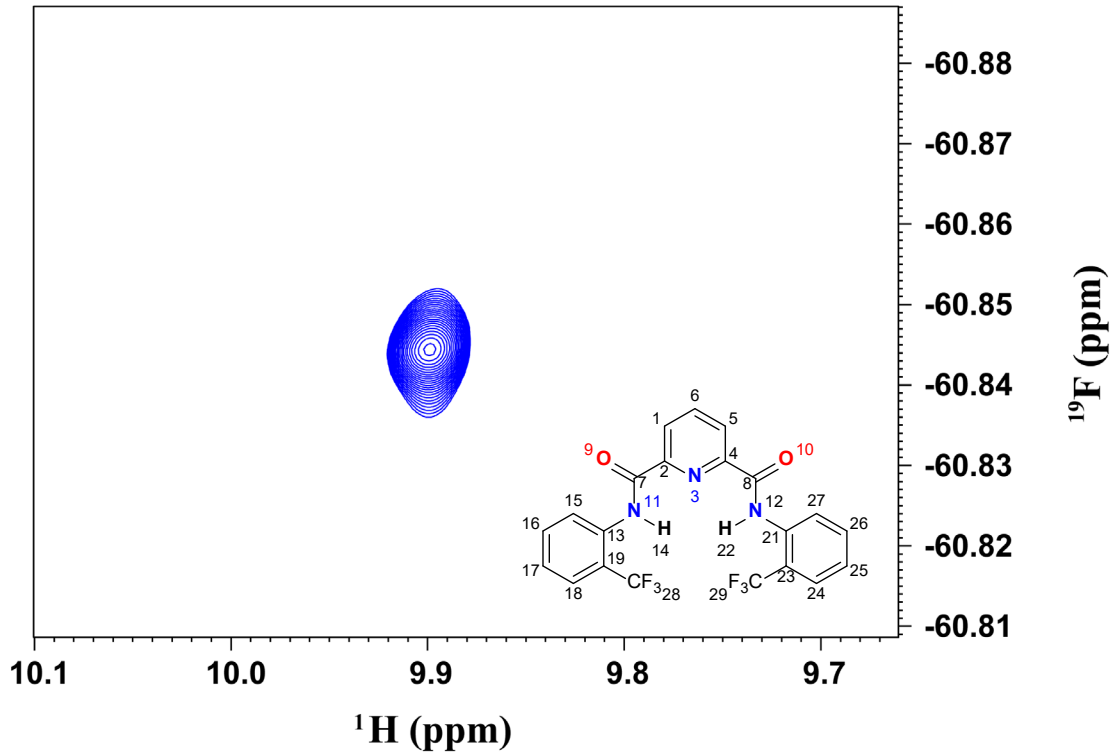

Figure S49: 2D ^{1}H-^{19}F HOESY spectrum of B4 molecule in $CDCl_3$ solvent

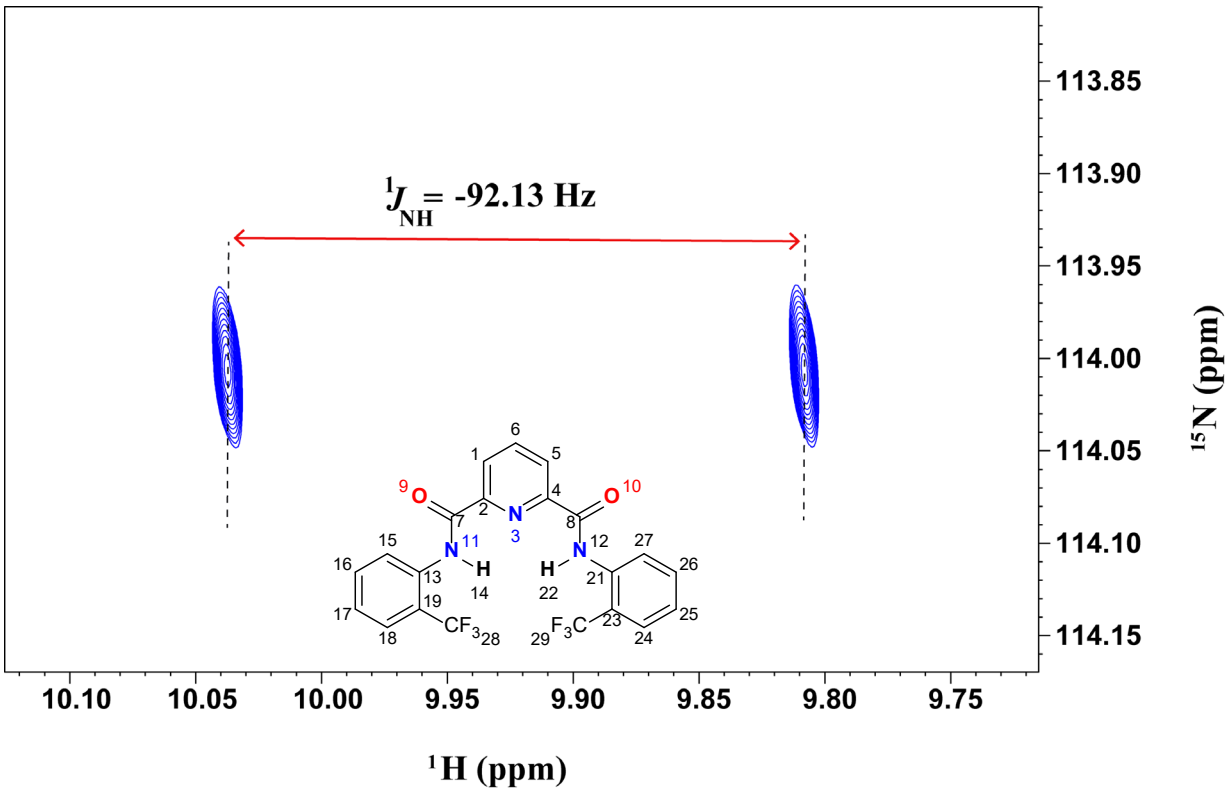

Figure S50: ^{1}H-coupled 2D ^{1}H-^{15}N HSQC spectrum of B4 molecule in $CDCl_3$ solvent

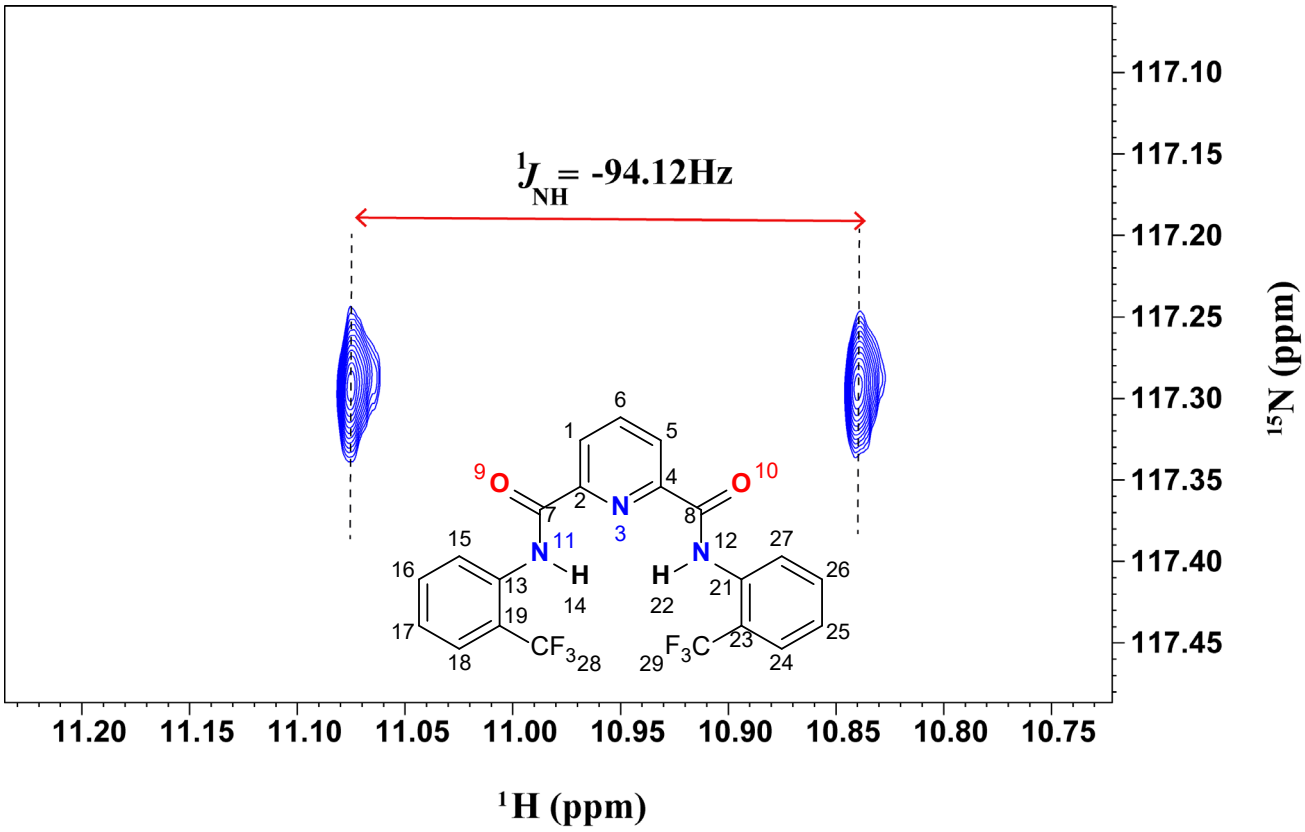

Figure S51: ^{1}H-coupled 2D ^{1}H-^{15}N HSQC spectrum of B4 molecule in DMSO-d_6 solvent

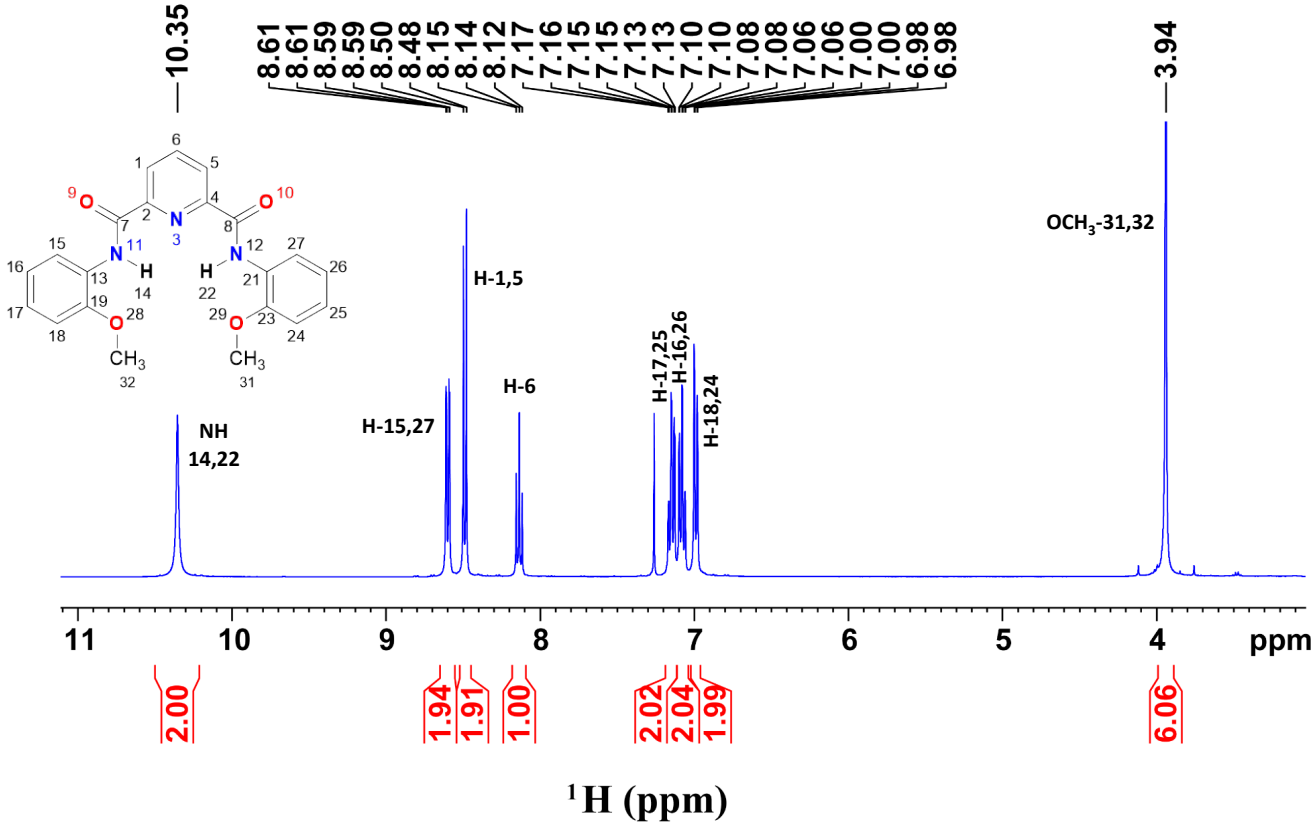

Figure S52: 400 MHz ^{1}H NMR spectrum of B5 molecule in $CDCl_3$ solvent

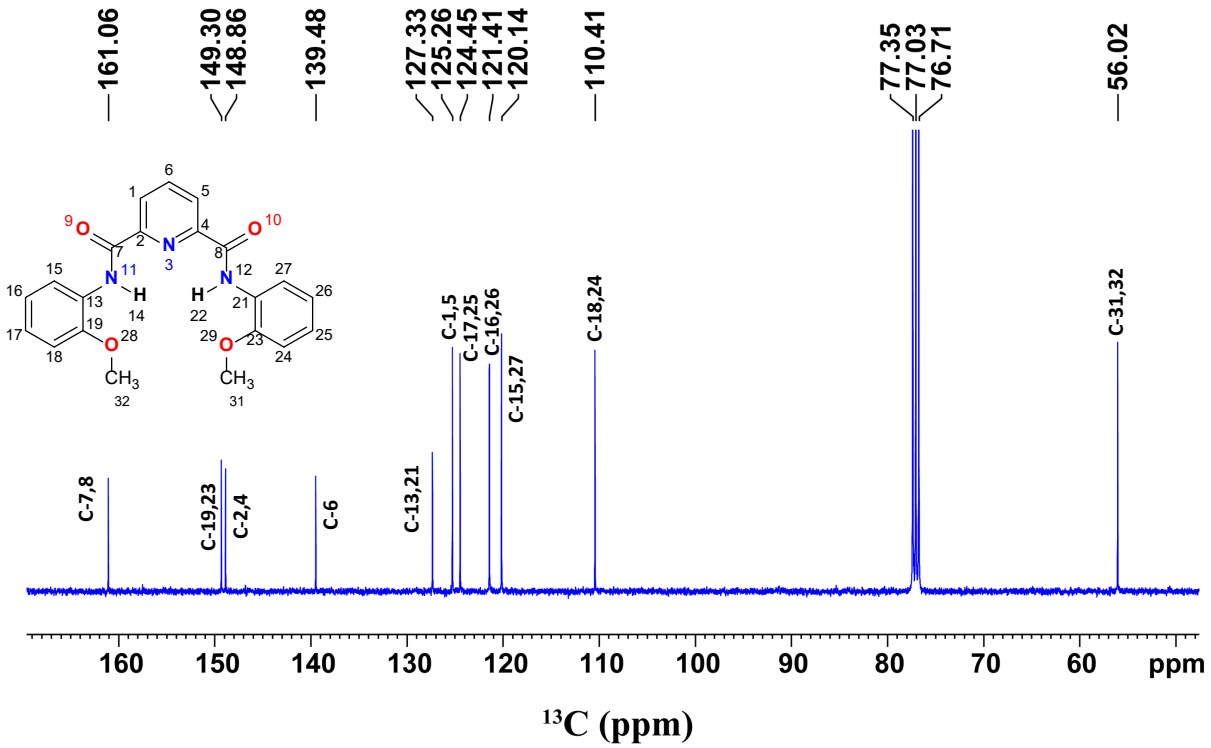

Figure S53: 100 MHz ^{13}C NMR spectrum of B5 molecule in $CDCl_3$ solvent

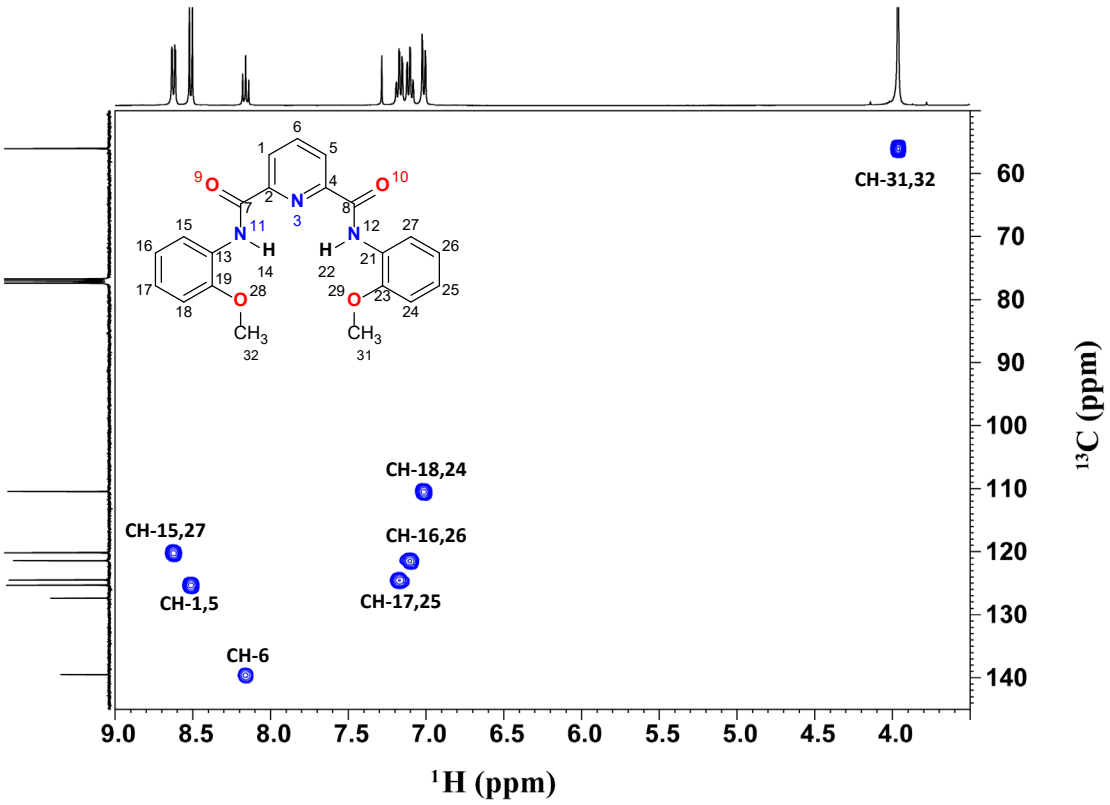

Figure S54: 2D ^{13}C-^{1}H HSQC spectrum of B5 molecule in $CDCl_3$ solvent

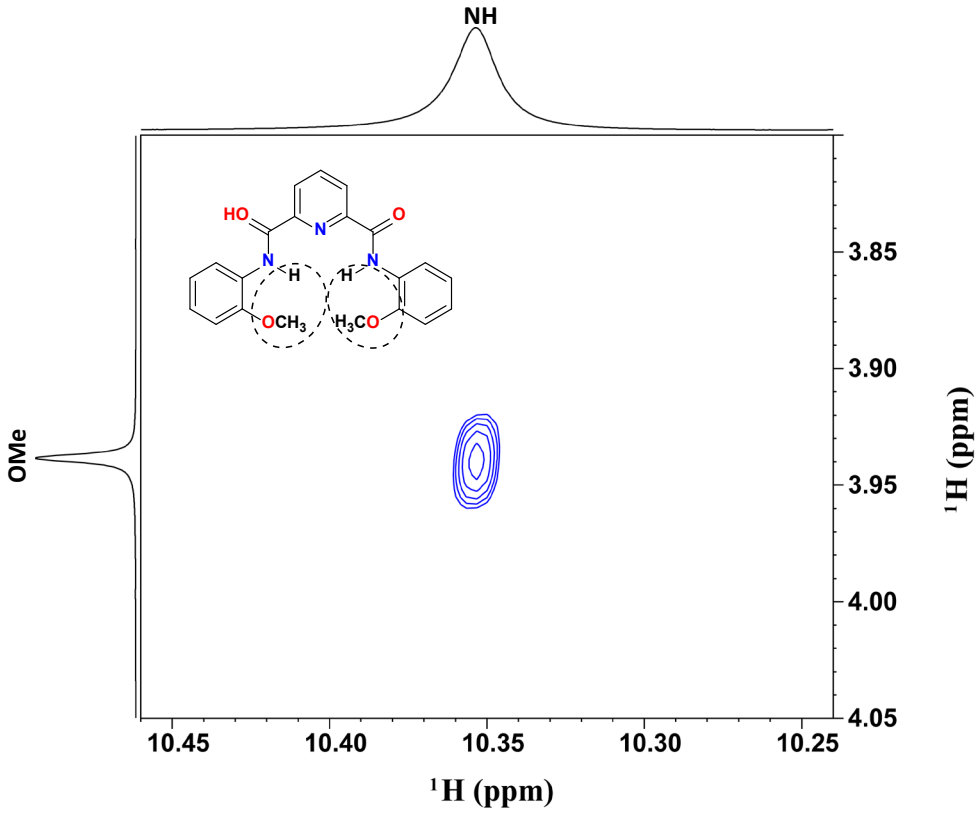

Figure S55: 2D NOESY spectrum of B5 molecule measured at 400 MHz in $CDCl_3$ solvent

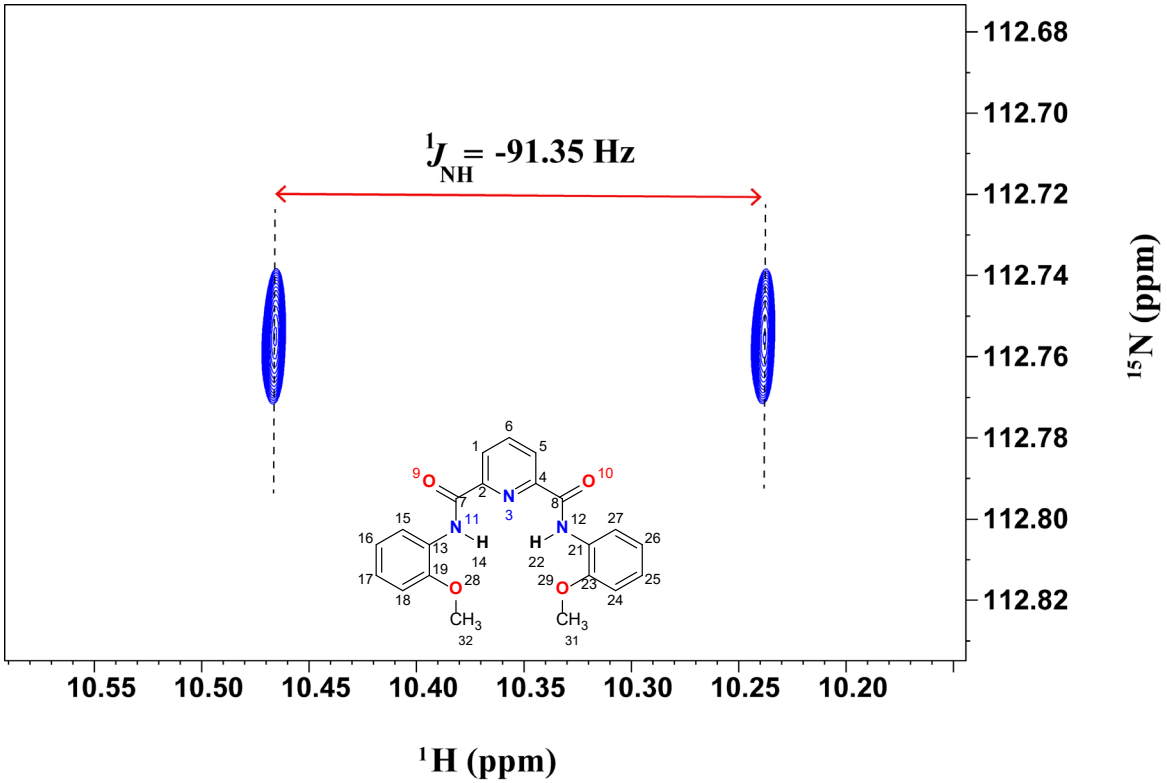

Figure S56: ^{1}H-coupled 2D ^{1}H-^{15}N HSQC spectrum of B5 molecule in $CDCl_3$ solvent

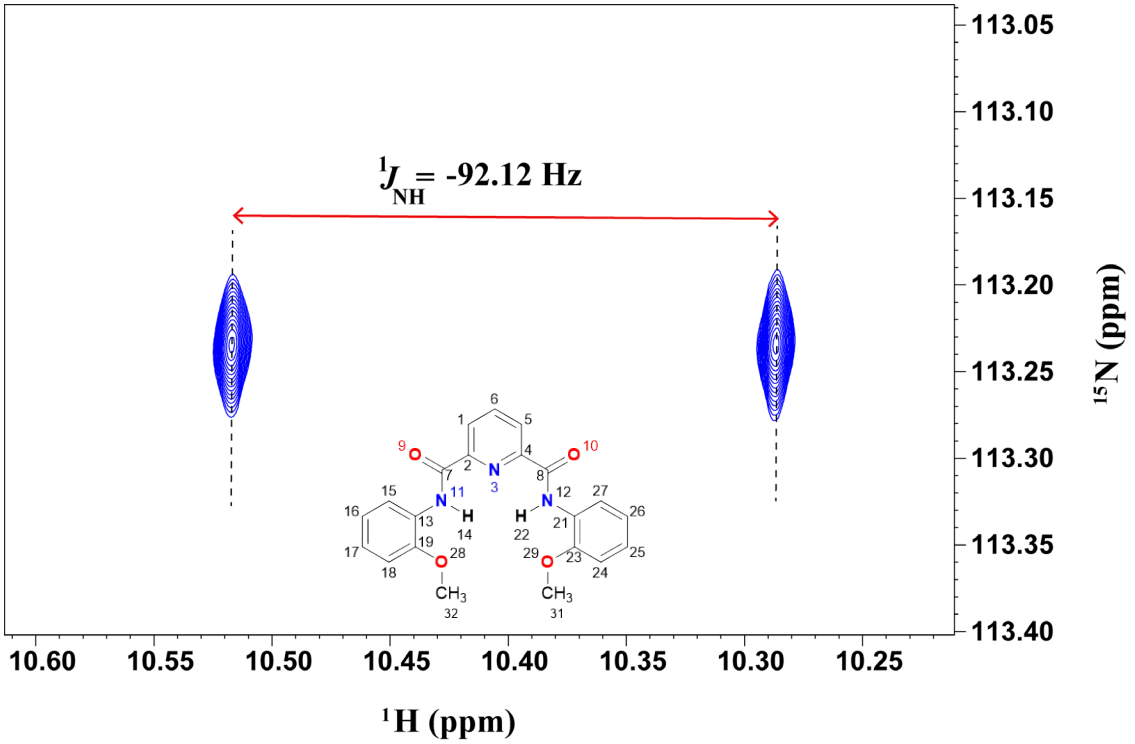

Figure S57: ^{1}H-coupled 2D ^{1}H-^{15}N HSQC spectrum of B5 molecule in DMSO-d_6 solvent

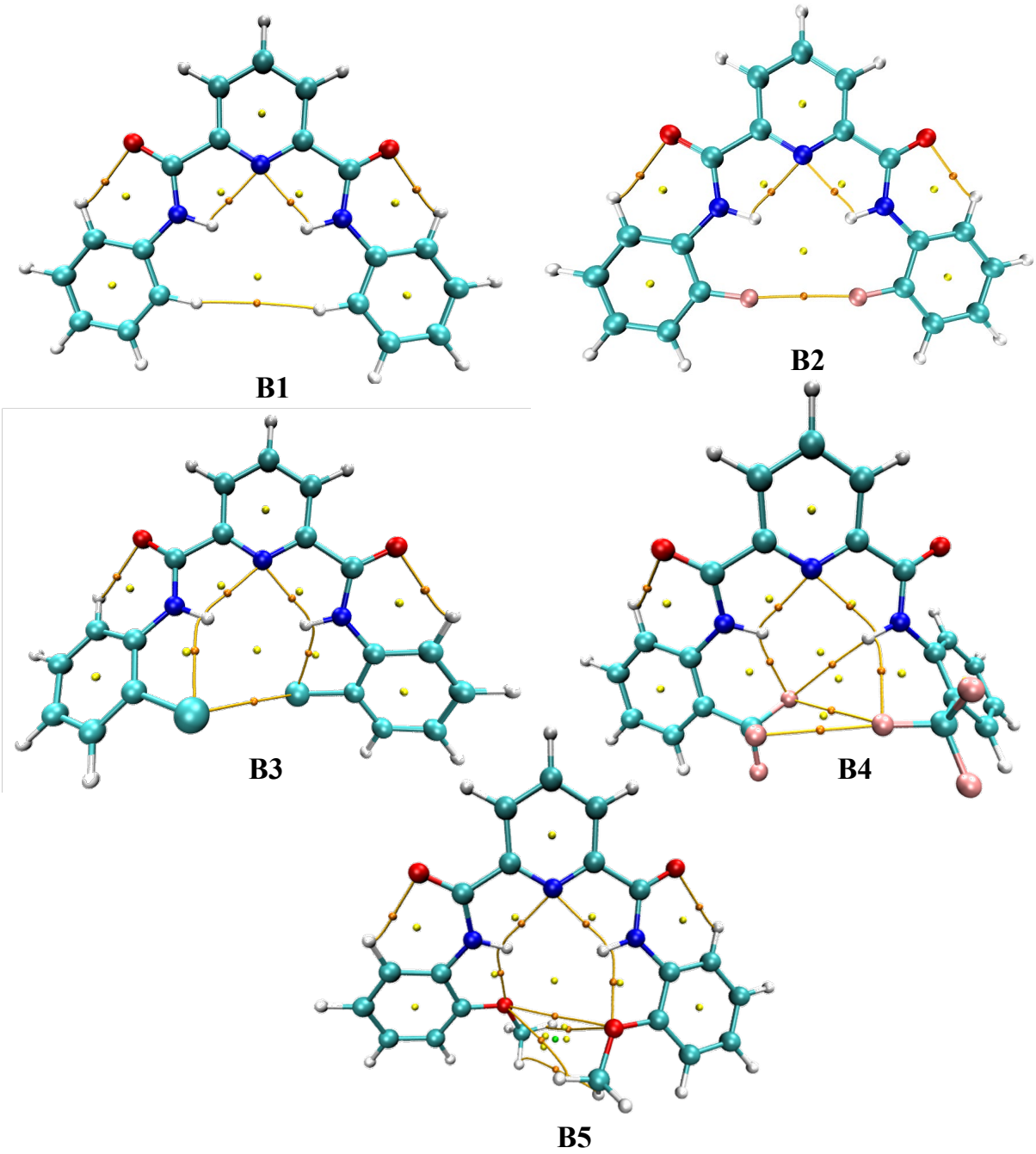

Figure S58: Visualization of (3, -1) BCPs and corresponding bond paths (BPs) associated with hydrogen bonding interactions for the B series of molecules (B1-B5) generated using B3LYP/6-311+G(d,p) optimized geometries.

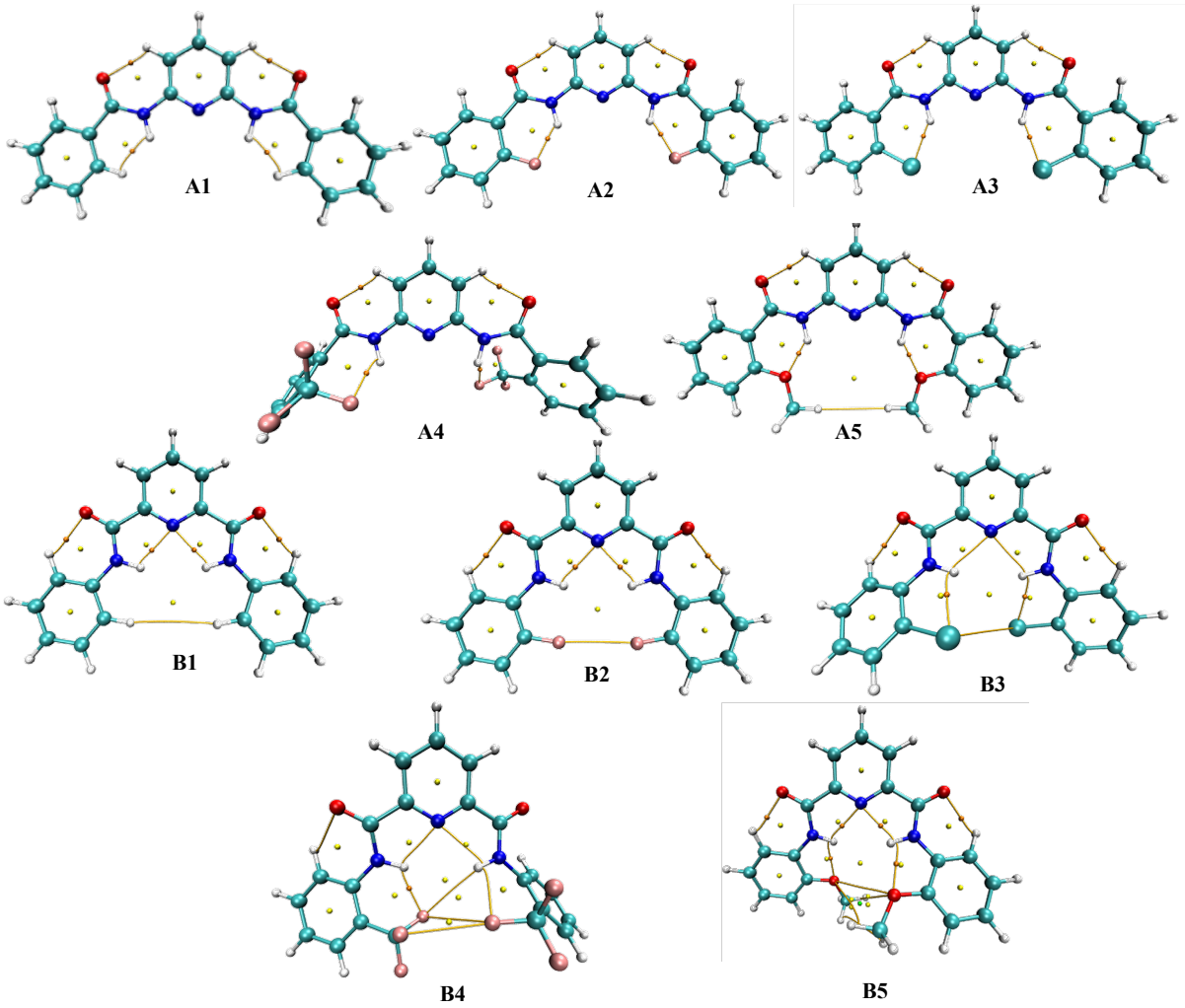

Figure S59: Visualization of (3, -1) BCPs and corresponding bond paths (BPs) associated with HBs for molecules A1-A5 and B1-B5 generated using B3LYP/6-311++G(d,p) optimized geometries. The dots representing the CPs, while thin yellow lines indicating the BPs of (3, -1) BCPs.

Non-covalent interaction: Series B

In the B series of molecules, three common intramolecular interactions are observed, *viz* C=O···H-Py, C=O···H-Ar, and H(N)···N-Py (Figure S59). In molecule B1, we can see three closely spaced spikes on the left side of the topology map, which are mainly attributed to these three interactions. In molecules B2 and B3, two additional spikes are observed due to the hydrogen bonding interaction of H(N)···X-C (X=F and Cl) and the van der Waals interaction between two halo atoms. For molecules B4 and B5, additional spikes are also observed alongside those mentioned above, corresponding to weak van der Waals interactions such as Ar–H···F–C in B4 and O-CH_3···H-Ar as well as CH_3-O···O-CH_3 in B5. The additional NCI spike associated with the NH···N-Py interaction in series B reflects increased conformational

locking and electronic redistribution, which directly impacts the availability and reactivity of the donor sites during complex formation.

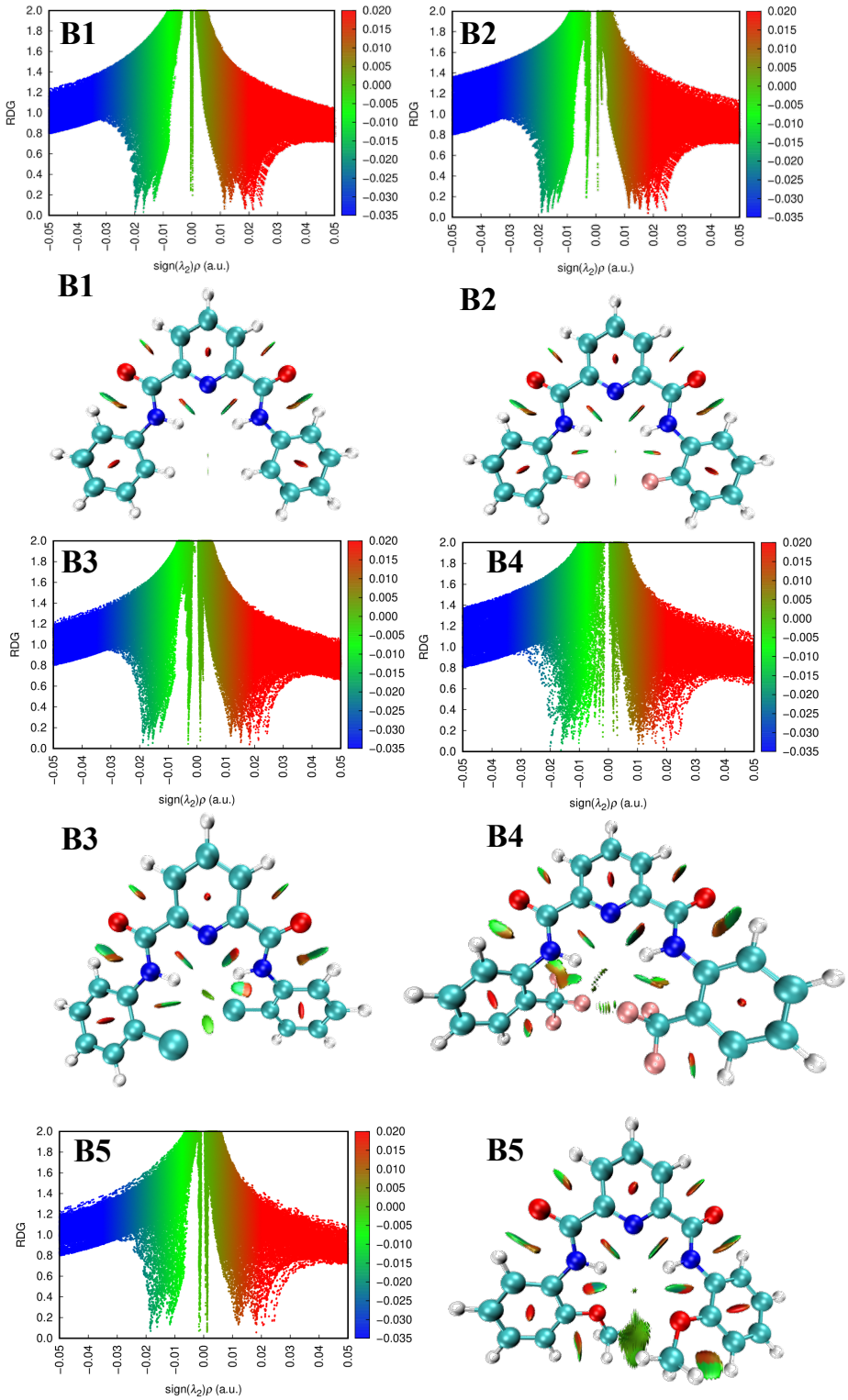

Figure S60: Plot of $sign(\lambda_2)\rho(r)$ vs RDG and corresponding color-filled isosurface maps for the B series of molecules (B1-B5) generated using geometries optimized at B3LYP/6-311+G(d,p) level of theory.

Non-covalent interaction: Series A and B geometries optimized at B3LYP/6-311++G(d,p)

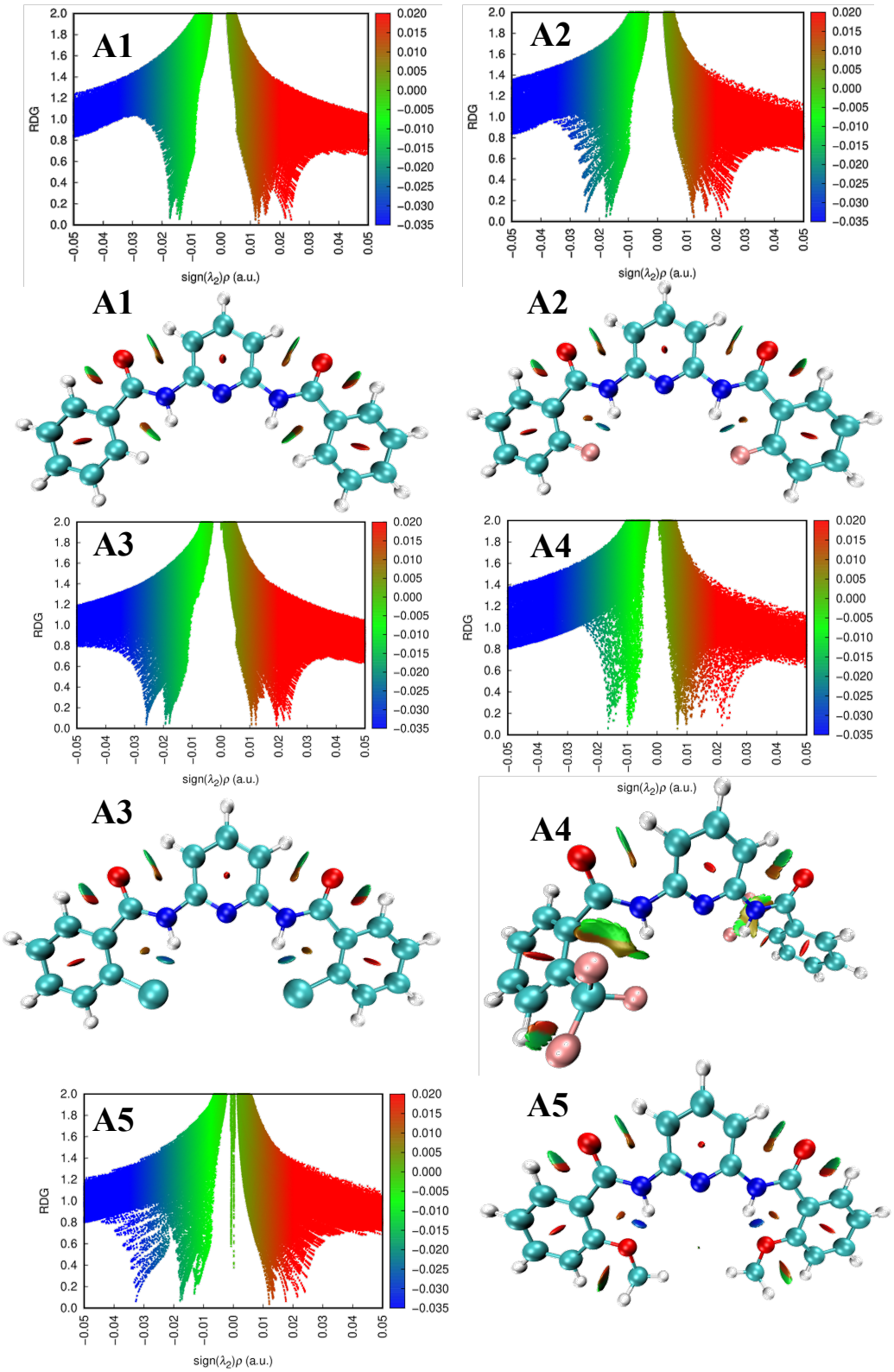

Figure S61: Plot of $sign(\lambda_2)\rho(r)$ vs RDG and corresponding color-filled isosurface maps for the molecules A1-A5 generated using geometries optimized at B3LYP/6-311++G(d,p) level of theory

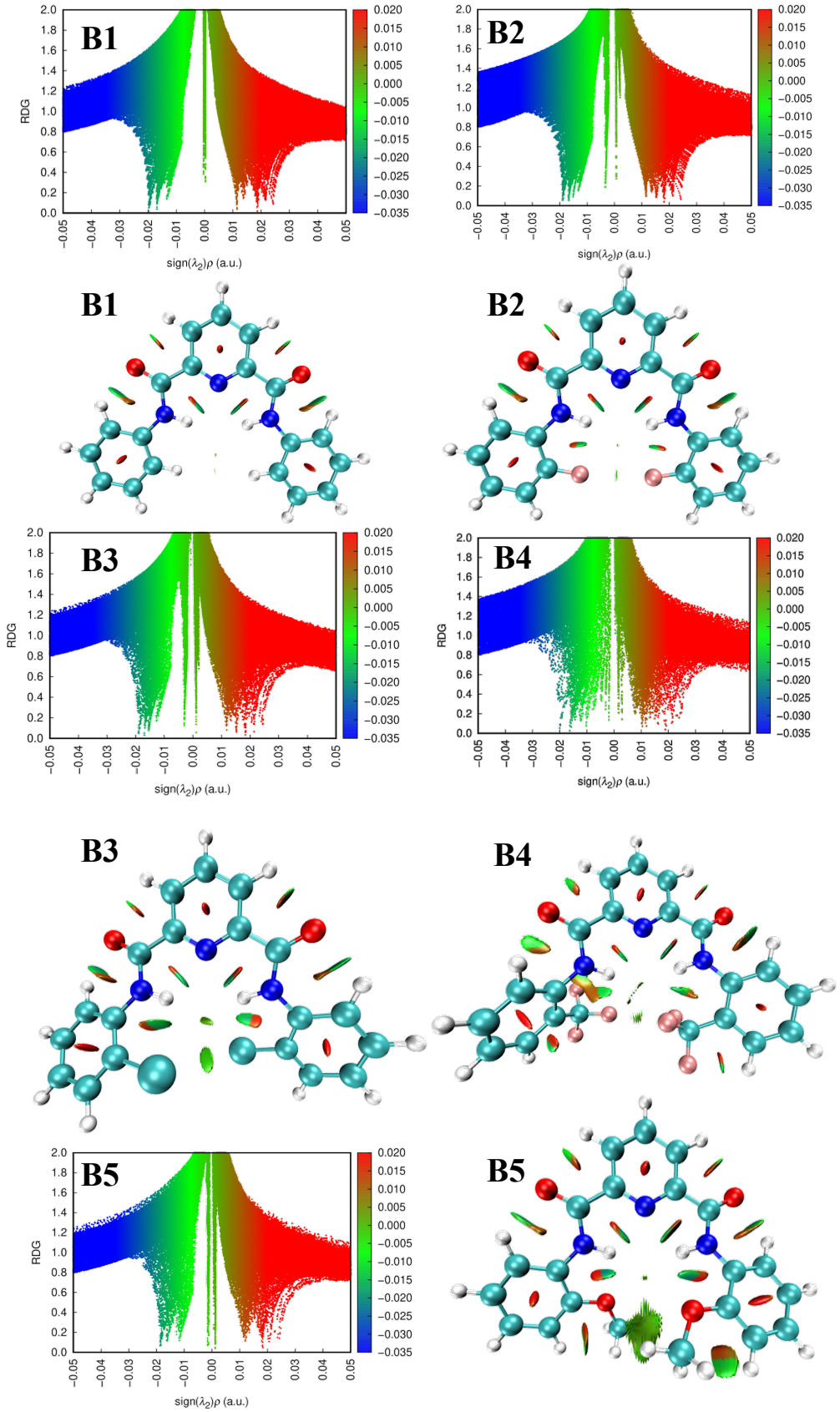

Figure S62: Plot of $sign(\lambda_2)\rho(r)$ vs RDG and corresponding color-filled isosurface maps for the molecules B1-B5 generated using geometries optimized at B3LYP/6-311++G(d,p) level of theory

Relaxed potential energy surface scan of A2, B2 and A4 molecules: Performed at B3LYP/6-311++G(d,p) level of theory.

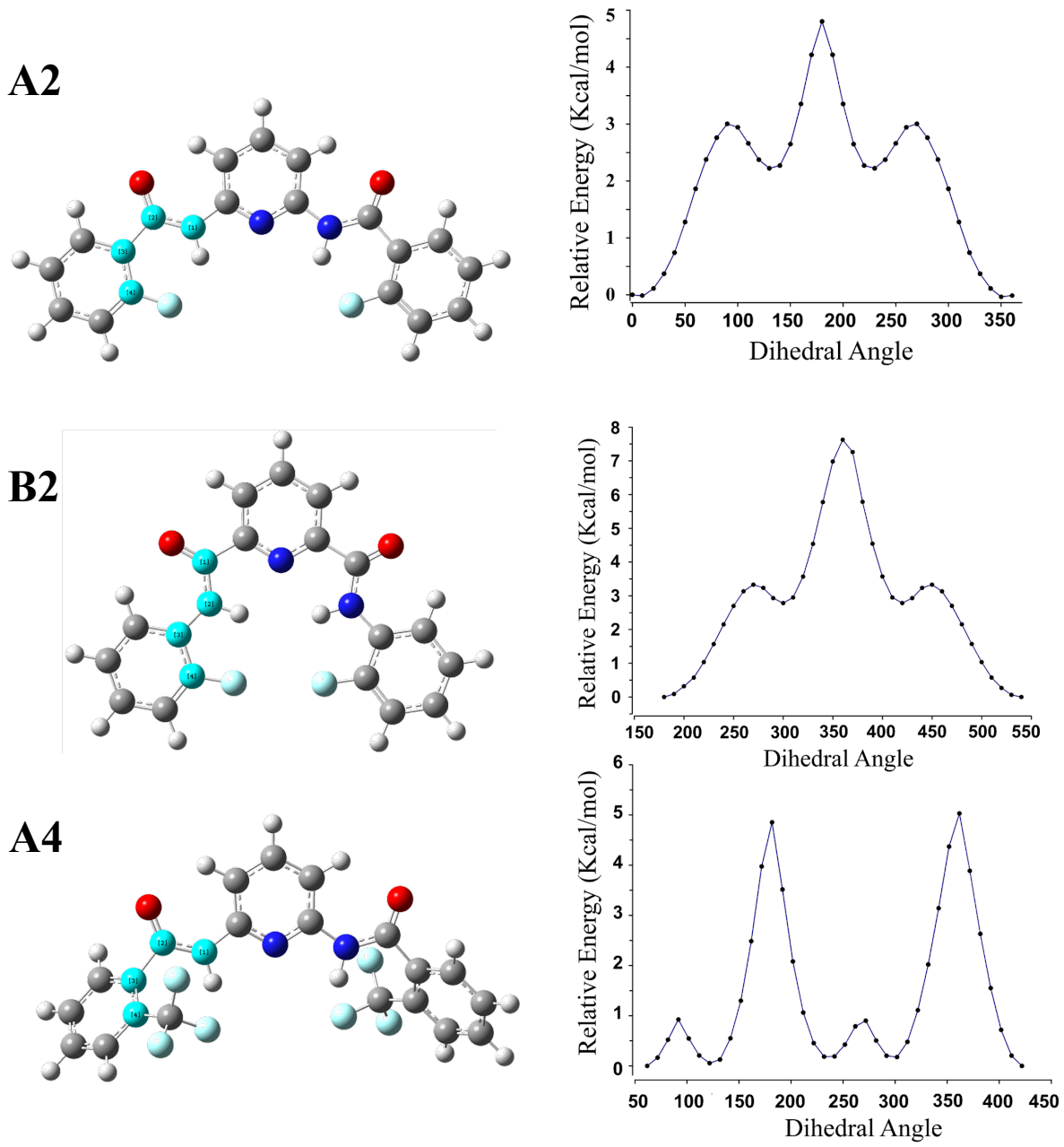

Figure S63: Relaxed PES of molecules A2, B2, and A4 for the internal rotation of the phenyl ring around the single bond. The selected atoms for scanning dihedral angles are highlighted in cyan color. The analysis was performed at B3LYP/6-311++G(d,p) level of theory.

References:

1. C. Yu and G. C. Levy, *J. Am. Chem. Soc.*, 1984, **106**, 6533-6537.
2. J. Battiste and R. A. Newmark, *Prog. Nucl. Magn. Reson. Spectrosc.*, 2006, **48**, 1-23.
3. G. Bodenhausen and D. J. Ruben, *Chem. Phys. Lett.*, 1980, **69**, 185-189.
4. M. J. Frisch, G. W. Trucks, H. B. Schlegel, G. E. Scuseria, M. A. Robb, J. R. Cheeseman, G. Scalmani, V. Barone, G. A. Petersson, H. Nakatsuji, X. Li, M. Caricato, A. V. Marenich, J. Bloino, B. G. Janesko, R. Gomperts, B. Mennucci, H. P. Hratchian, J. V. Ortiz, A. F. Izmaylov, J. L. Sonnenberg, Williams, F. Ding, F. Lipparini, F. Egidi, J. Goings, B. Peng, A. Petrone, T. Henderson, D. Ranasinghe, V. G. Zakrzewski, J. Gao, N. Rega, G. Zheng, W. Liang, M. Hada, M. Ehara, K. Toyota, R. Fukuda, J. Hasegawa, M. Ishida, T. Nakajima, Y. Honda, O. Kitao, H. Nakai, T. Vreven, K. Throssell, J. A. Montgomery Jr., J. E. Peralta, F. Ogliaro, M. J. Bearpark, J. J. Heyd, E. N. Brothers, K. N. Kudin, V. N. Staroverov, T. A. Keith, R. Kobayashi, J. Normand, K. Raghavachari, A. P. Rendell, J. C. Burant, S. S. Iyengar, J. Tomasi, M. Cossi, J. M. Millam, M. Klene, C. Adamo, R. Cammi, J. W. Ochterski, R. L. Martin, K. Morokuma, O. Farkas, J. B. Foresman and D. J. Fox, *Gaussian 16 Rev. C.01*, (2016), Wallingford, CT.
5. E. Cancès, B. Mennucci and J. Tomasi, *J. Chem. Phys.*, 1997, **107**, 3032-3041.
6. K. Wolinski, J. F. Hinton and P. Pulay, *J. Am. Chem. Soc.*, 1990, **112**, 8251-8260.
7. D. Kumar Singh Khaidem, S. A. Shimray, A. Ningthoujam, S. Begum, F. A. S. Chipem and G. Krishnamoorthy, *J. Mol. Liq.*, 2024, **394**, 123765.
8. S. Gatfaoui, N. Issaoui, A. Mezni, F. Bardak, T. Roisnel, A. Atac and H. Marouani, *J. Mol. Struct.*, 2017, **1150**, 242-257.